Molecular Diversity
https://doi.org/10.1007/s11030-020-10112-3

ORIGINAL ARTICLE

Synthesis, antimicrobial evaluation, and in silico studies of quinoline—1*H*-1,2,3-triazole molecular hybrids

Paul Awolade[1] · Nosipho Cele[1] · Nagaraju Kerru[1] · Parvesh Singh[1]

Received: 3 March 2020 / Accepted: 27 May 2020

Abstract

Antimicrobial resistance has become a significant threat to global public health, thus precipitating an exigent need for new drugs with improved therapeutic efficacy. In this regard, molecular hybridization is deemed as a viable strategy to afford multi-target-based drug candidates. Herein, we report a library of quinoline—1*H*-1,2,3-triazole molecular hybrids synthesized via copper(I)-catalyzed azide-alkyne [3 + 2] dipolar cycloaddition reaction (CuAAC). Antimicrobial evaluation identified compound **16** as the most active hybrid in the library with a broad-spectrum antibacterial activity at an MIC_{80} value of 75.39 µM against methicillin-resistant *S. aureus*, *E. coli*, *A. baumannii,* and multidrug-resistant *K. pneumoniae*. The compound also showed interesting antifungal profile against *C. albicans* and *C. neoformans* at an MIC_{80} value of 37.69 and 2.36 µM, respectively, superior to fluconazole. In vitro toxicity profiling revealed non-hemolytic activity against human red blood cells (hRBC) but partial cytotoxicity to human embryonic kidney cells (HEK293). Additionally, in silico studies predicted excellent drug-like properties and the importance of triazole ring in stabilizing the complexation with target proteins. Overall, these results present compound **16** as a promising scaffold on which other molecules can be modeled to deliver new antimicrobial agents with improved potency.

Graphic abstract

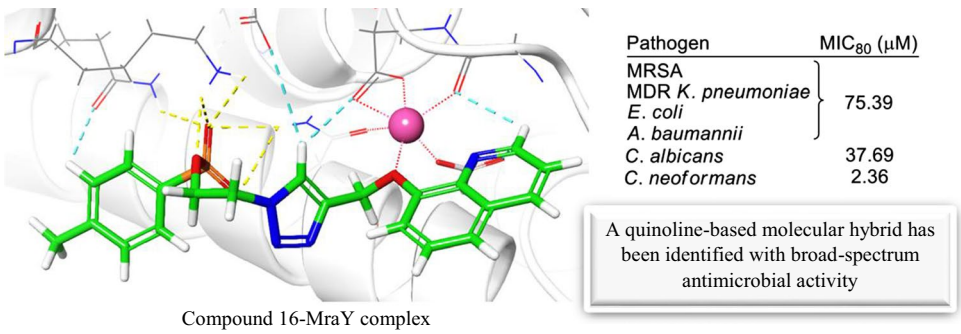

Compound 16-MraY complex

Keywords Antimicrobial resistance · Molecular hybridization · Quinoline · 1*H*-1,2,3-triazole · In silico

Introduction

The world today is burdened with an increasing number and widespread emergence of drug-resistant pathogens, which puts man's existence at risk. Despite the laudable progress made in antimicrobial drug research, the witty evolutions in the drug-resistance machinery of pathogenic microbes have stayed abreast of man's ingenuity. Infections that were once curable with single or combination therapies are now

Electronic supplementary material The online version of this article (https://doi.org/10.1007/s11030-020-10112-3) contains supplementary material, which is available to authorized users.

✉ Parvesh Singh
singhp4@ukzn.ac.za; parveshdurban@gmail.com

[1] School of Chemistry and Physics, University of KwaZulu-Natal, P/Bag X54001, Westville, Durban, South Africa

Published online: 07 June 2020

insidiously elusive to control even as the likelihood of drug-resistant infections compromises the outcome of invasive surgeries [1]. The upsurge in the cost of medical care and the rising rates of morbidity and mortality due to this menace also stifles effective clinical practice [2, 3]. Therefore, the development of new antimicrobial agents is indispensable to effective disease control.

Target-based approach has been widely employed in drug discovery over the years [4]. However, in recent times, multi-target-drug design (MTDD) strategies are favored over conventional single-target-based drugs owing to the propensity of pathogens to mutate or bypass susceptible drug targets [5]. As a result, molecular hybridization (MH) has gained increased attention as an MTDD strategy since it allows the incorporation of two or more bioactive scaffolds into a molecular entity, which subsequently displays multiple-receptor recognition and an improved therapeutic effect [6].

The preference of MH in drug design thrives on the easy access to linkers and spacers explored in assembling the hybrid molecules. In this regard, the 1*H*-1,2,3-triazole ring has proven to be exceptional thanks to its broad bioactivity spectrum [7–9], resistance to biodegradation in vivo, and bioisosterism of amide, *trans*-olefinic, carboxylic acid moiety, and ester units [10]. The hydrogen bonding (H-b) ability of the ring nitrogen and H-5' atoms for multiple-binding to drug targets also encourage its utility in drug design. For instance, a quinoline-1*H*-1,2,3-triazole hybrid exhibited 909- and 364-fold superior anticandidal efficacy compared to the parent 8-hydroxyquinoline and fluconazole [11, 12]. The antimicrobial profile of 1*H*-1,2,3-triazole hybrids of ciprofloxacin-based drugs was also enhanced by up to 69-fold compared to the parent drugs [13–16]. Precisely, the moxifloxacin-triazole hybrid showed twofold superior inhibition of DNA-gyrase compared to moxifloxacin and gatifloxacin [17].

Quinoline is another prominent pharmacophore found in many bioactive natural products and synthetic molecules. A distinct class of this heterocycle, 8-hydroxyquinoline (8-HQ), and its derivatives (Fig. 1) are privileged scaffolds with an excellent metal chelating property that confers desirable therapeutic potentials [18, 19]. Nevertheless, toxicity burdens limit their clinical utility, for example the withdrawal of the oral form of clioquinol, an antiparasitic agent. The observed toxicity is partly due to the hydroxy unit's susceptibility to phase II metabolism via glucuronidation pathway, subsequent enterohepatic circulation, and possible *β*-glucuronidase-mediated release of the active form in areas with high expression of the glycosyl hydrolase [20, 21]. Therefore, we envisage that the *O*-conjugation of 8-HQ will attenuate its toxicity drawback while affording molecules with desired antimicrobial activity.

Based on the foregoing, the present work describes the synthesis of a library of quinoline—1*H*-1,2,3-triazole hybrids as a continuation of our research on the development of antimicrobial agents with an improved pharmacological profile using the MH approach [22, 23]. The molecular design incorporates an alkane spacer bearing terminal *O* and *NH* units to improve lipophilicity and H-b potential, respectively. Potent compounds (% inhibition ≥ 80) were further examined for their in vitro cytotoxicity and hemolytic activities against human embryonic kidney cells (HEK293) and human red blood cells (hRBC), respectively. Also, in silico techniques were used to predict the drugability of potent compounds and their binding profiles with selected drug targets to rationalize their antimicrobial activities.

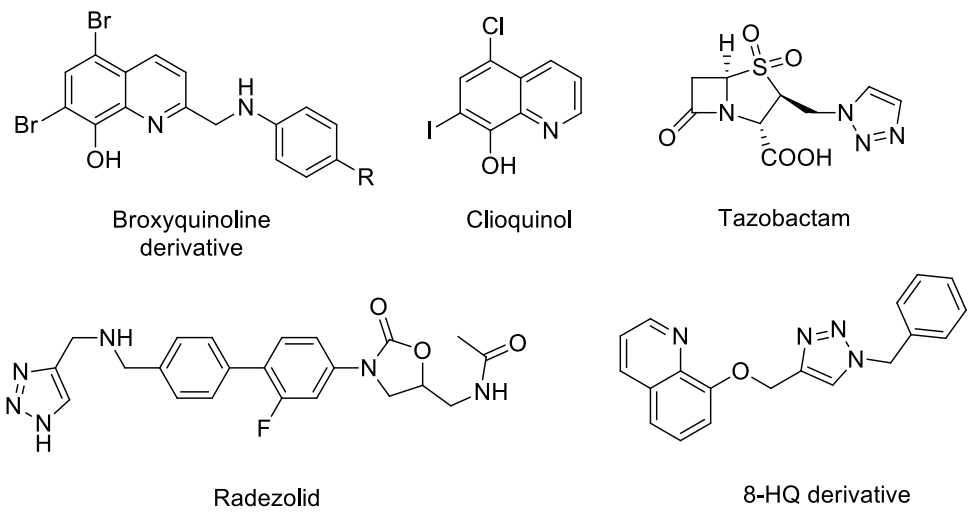

Fig. 1 Antimicrobial agents bearing 8-hydroxyquinoline and 1*H*-1,2,3-triazole units

Results and discussion

Chemistry

The synthetic protocol began with the preparation of required azide fragments according to their substrate demands (Scheme 1). HCl/$NaNO_2$-mediated diazotization of substituted anilines and subsequent treatment of the resulting diazonium salt with NaN_3 gave phenyl azides **1a–u** in moderate to quantitative yields. (2-azidoethoxy) benzenes **3a–z** were obtained by refluxing phenols with 1,2-dibromoethane in 25% NaOH solution containing *tert*-butylammonium bromide (TBAB), followed by heating the bromoethyl intermediates (**2a–z**) with NaN_3 to give azides **3a–z** in over 70% overall yield. Notably, omitting TBAB increased both the reaction time for **2a–z** and the quantity of undesired *bis*-products. The preparation of **7a–n** akin to **3a**–**z** was, however, unsuccessful. Hence, azidation of 2-chloroethanol in water was performed first, followed by tosylation of the resulting 2-azidoethanol (**5**) to give 2-azido-*O*-ethyl tosylate (**6**). *N*-alkylation of substituted anilines with compound **6** then afforded azides **7a–n** in over 50% yield. The phenol and aniline precursors of azide **3j**, **3t–v,** and **7g** were prepared according to the literature [24, 25].

On the other hand, the alkyne fragment, compound **8**, was synthesized in 93% yield from a base-promoted *O*-alkylation of commercially available **8-HQ** with propargyl bromide (Scheme 2). Then, copper(I)-catalyzed azide-alkyne [3 + 2] dipolar cycloaddition reaction (CuAAC) afforded the target hybrids **9a**–**u**, **10a**–**z,** and **11a**–**n** in moderate to excellent yields. Compounds **14**–**18** were also prepared for SAR studies to examine the influence of *O*- or *NH*-linked alkane spacer and triazole ring on antimicrobial activity (Scheme 3). The synthesized compounds were characterized using spectroscopic techniques, i.e., FT-IR, HRMS, and NMR (^{1}H, ^{13}C, and 2D).

Structural elucidation

The conversion of azides to triazoles was depicted in the FT-IR spectra of target hybrids by the disappearance of strong and sharp absorption bands for azido ($-N=N^+=N^-$) and alkynyl (≡C–H) stretching vibrations around 2090–2100 cm^{-1} and 3275 cm^{-1}, respectively. The bands for C≡C stretching at 2121 cm^{-1} and ≡C–H deformation at 700–600 cm^{-1} were also absent. Furthermore, the exclusive formation of 1,4-disubstituted 1*H*-1,2,3-triazole ring was confirmed by NMR spectroscopy. In the ^{1}H NMR spectra, the terminal alkyne resonances and allylic couplings, i.e., the triplet peak of $-C\equiv CH$ at δ_H 2.54 ($^4J = 2.4$ Hz) and doublet peak of $-OCH_2$ at δ_H 5.03

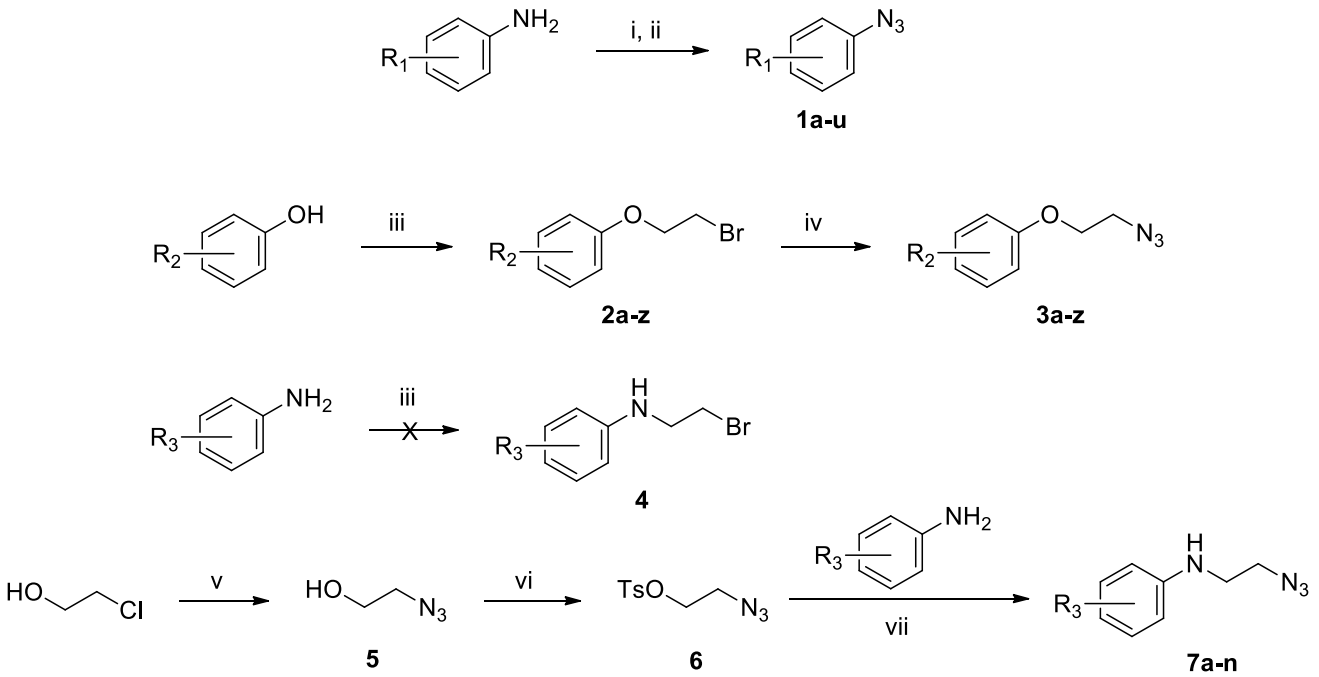

Scheme 1 Synthetic route to azide fragments. Reagents and conditions: (i) HCl: H_2O (1:1), $NaNO_2$, 0 °C, 30 min, (ii) NaN_3, 0 °C to RT, 2 to 3 h. 60–100% yield over two steps, (iii) 25% NaOH, 1,2-dibromoethane, TBAB, 80 °C, 5–12 h, (iv) NaN_3, DMF, 80 °C, 30 min to 1 h, > 70% overall yield, (v) NaN_3, H_2O, 90 °C, 18 h, (vi) *p*-TsCl, Et_3N, DCM, 0 °C to RT, 16 h, 66% yield, (vii) $CaCO_3$, KI, acetone: H_2O (1:1), 50–70% yield

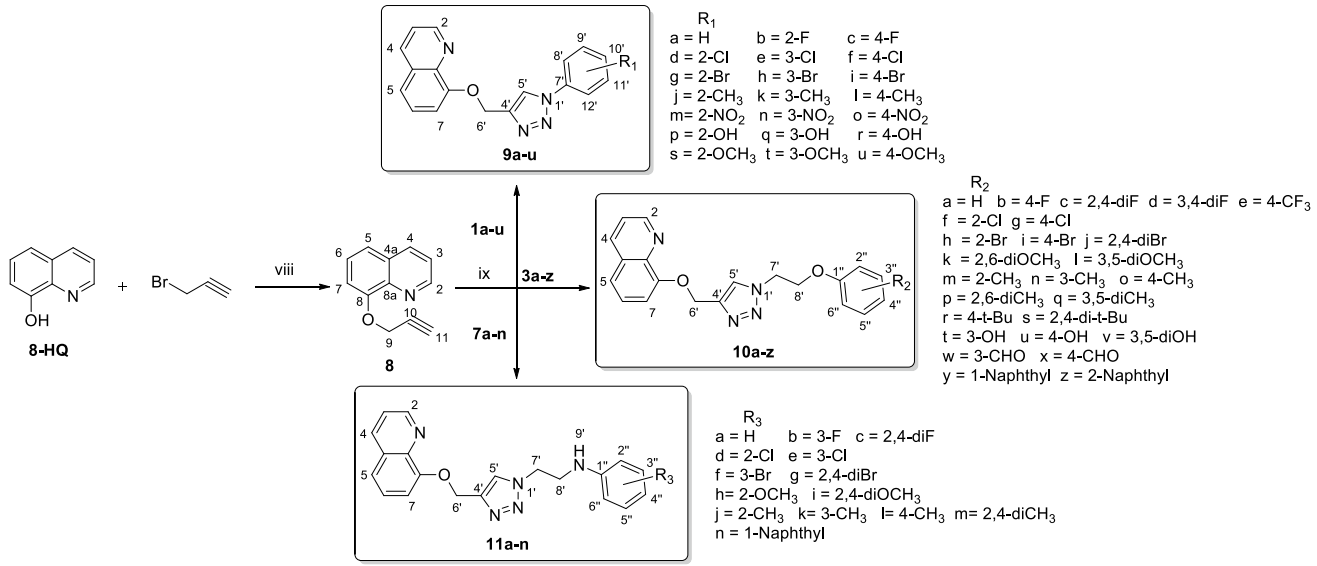

Scheme 2 Synthetic route to target hybrids. Reagents and conditions: **(viii)** anhydrous K_2CO_3, DMF, RT, 4 h, 93%. **(ix)** appropriate azides, DCM: H_2O (1:1), $CuSO_4.5H_2O$, sodium ascorbate, RT, 2 to 4 h

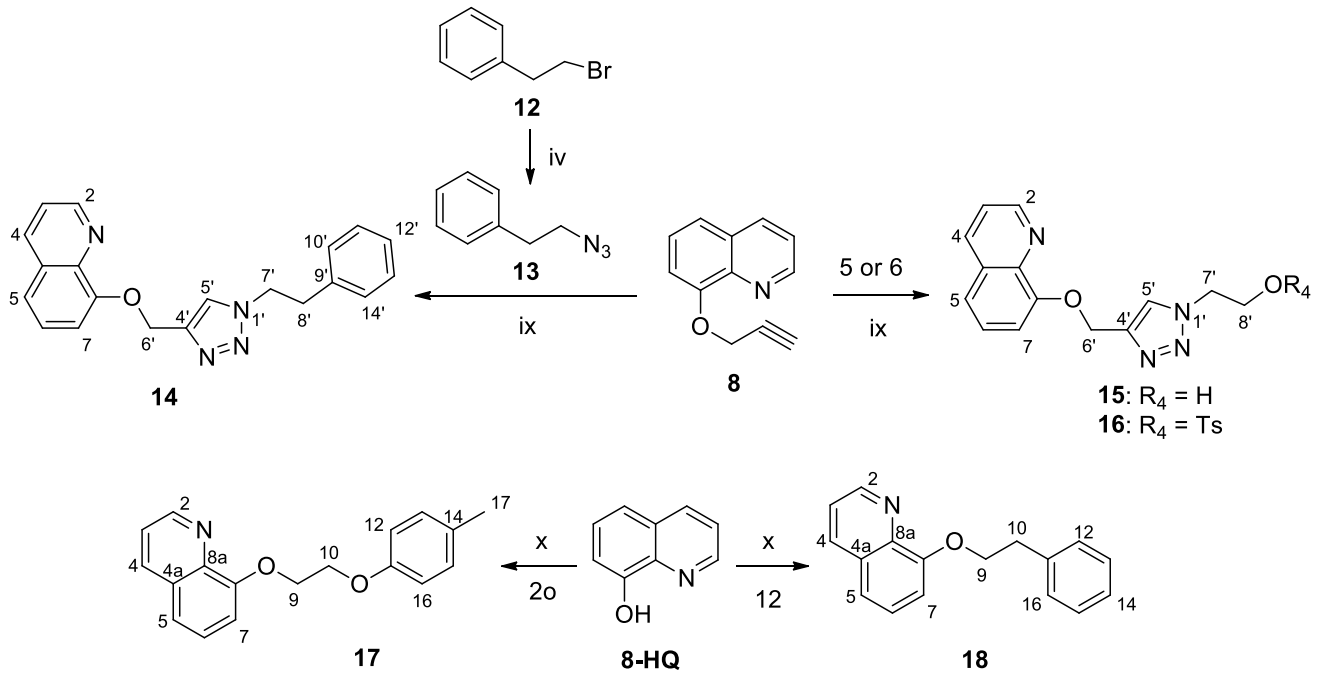

Scheme 3 Synthesis of compounds for SAR studies. Reagents and conditions: **(iv)** NaN_3, DMF, 80 °C, 30 min, quantitative yield, **(ix)** DCM: H_2O (1:1), $CuSO_4.5H_2O$, sodium ascorbate, RT, 2 h, 50–90% yield, **(x)** anhydrous K_2CO_3, DMF, 80 °C, 1 h, ~90% yield

($^4J = 2.4$ Hz), respectively, were absent, while a prominent singlet peak for H-5' of triazole ring appeared at δ_H 8.10 − 8.90 (**9a**–**u**), 7.85–8.37 (**10a**–**z**), and 7.71–7.85 (**11a**–**n**). The corresponding alkynyl $-C\equiv CH$ signals at δ_C 78.30 and 76.08 were also absent in the ^{13}C spectra, while *C*-4' and *C*-5' resonances of triazole ring were observed at δ_C 140–145 and 121–125, respectively. Interestingly, in the ^1H NMR spectrum of phenyl hybrid **9b**, the H-b ability of triazole H-5' atom was evidenced by a doublet peak at δ_H 8.29 ($^5J_{HF} = 2.6$ Hz) due to ^{19}F coupling. A corresponding doublet signal at δ_C 125.20 for C-5' ($^4J_{CF} = 3.9$ Hz) was also observed in the ^{13}C spectrum.

The successful hybridization of quinoline and 1*H*-1,2,3-triazole was further confirmed with 2D-NMR data. For example, the heteronuclear multiple bond coherence (HMBC) spectrum for compound **16** (depicted in Fig. 2) showed HMBC correlations of H-5' (δ_H 7.85, 1H, s) to C-4' (δ_C 144.28) and C-7' (δ_C 49.09); H-6' (δ_H 5.51, 2H, s) to C-8 (δ_C 153.81), C-4' (δ_C 144.28) and C-5' (δ_C 124.39); as well as H-7' (δ_H 4.60, 2H, t) to C-5' (δ_C 124.39) and C-8' (δ_C 67.32). Moreover, a prominent molecular ion peak at $m/z = (M + Na)^+$ in the high-resolution mass spectrum of target hybrids validated the established structures.

Antimicrobial studies

The antimicrobial potential of quinoline–1*H*-1,2,3-triazole hybrids, compounds **14**–**18** and their precursor (**8-HQ**), was examined against ESKAPE pathogens, viz. MRSA (ATCC 43300), MDR *K. pneumoniae* (ATCC 700603), *E. coli* (ATCC 25922), *A. baumannii* (ATCC 19606), and *P. aeruginosa* (ATCC 27853) as well as two fungi: *C. albicans* (ATCC 90028) and *C. neoformans* (ATCC 208821). A uniform test concentration of 32 µg/mL was used for the whole-cell growth inhibition assays. Subsequently, potent hybrids, i.e., those providing ≥ 80% inhibition of pathogen's growth, were re-evaluated in a dose–response assay to determine their minimum inhibitory concentration (MIC_{80}).

The results presented in Table 1 show that the molecular hybrids exhibit activity profiles similar to their precursor **8-HQ**, i.e., stronger efficacy as antifungal agents. However, moderate antibacterial activities were found with compound ***9l*** (79.6% growth inhibition of *A. baumannii* at 101.15 µM; 32 µg/mL) and compound **10v** (MIC_{80} = 84.57 µM against MRSA). Other compounds did not show ≥ 80% inhibition of selected bacteria strains at the maximum tested concentration (32 µg/mL). Antifungal activity was conserved with methyl, hydroxy, and 2-chloro substituted hybrids. The most active phenyl hybrid **9q** (MIC_{80} = 12.57 µM) exhibited two-fold stronger anticryptococcal activity than the reference drug fluconazole, whereas compounds **10d**, **10v,** and **10z** showed equipotent anticryptococcal activities with an MIC_{80} value around 20 µM. Moreover, the superior activity profile

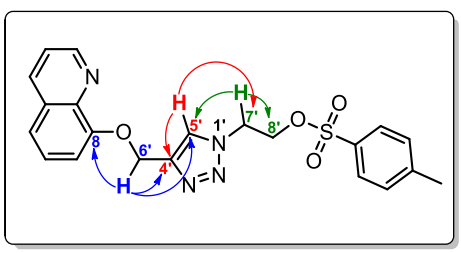

Fig. 2 Key HMBC correlations in compound 16

of phenoxy hybrids compared to anilino hybrids partly suggests the preference of H-b acceptor over H-b donor.

The importance of *O* or *NH*-linked alkane spacer, triazole core, and phenyl ring to antifungal activity was established from an analysis of the structure–activity relationship (SAR) of target hybrids and compounds **14**–**19**. For instance, both compounds **9a** and **14**, which lacks the alkane spacer, were inactive compared to phenoxy and anilino hybrid **10a** and **11a**, respectively, with moderate activities. The activity of compound **10a** and inactivity of compound **15** also reveal the significance of phenyl unit to lipophilicity.

Furthermore, the significance of 1*H*-1,2,3-triazole core to antimicrobial activity and its synergy with alkane spacer and sulfone unit is evidenced by the broad-spectrum antimicrobial potency of compound **16**. The compound emerged as the most potent antimicrobial agent overall. With an MIC_{80} value of 75.39 µM, compound **16** displayed several-fold superior antibacterial potency compared to compounds **15**, **18, 19,** and **8-HQ** against the Gram-negative pathogens. Compound **16** is also the only promising inhibitor of *P. aeruginosa,* with 64.8% inhibition at 75.39 µM (32 µg/mL). Although the compound is less potent than the single-spectrum antibacterial agents, colistin, and vancomycin, the structure can serve as a good starting point to develop broad-spectrum antibacterial agents with increased potency. Moreover, compound **16** showed an MIC_{80} value of 2.36 µM against *C. neoformans*, which is 11-fold stronger than fluconazole. This superior anticryptococcal activity might be due to the compound's increased lipophilicity, which will favor cellular membrane penetration for effective inhibition of fungal growth [26].

Cytotoxicity and hemolytic activity

Toxicity evaluation remains the crux of drug development and the primary cause of failure for many drug candidates in clinical trials [27]. The therapeutic safety of a drug is its ability to exert the desired physiological response without harmful effects on normal cellular structure and functions. A significant difference between the efficacious and toxic dose is therefore of uttermost importance.

The cytotoxicity and hemolytic profiles of potent hybrids were determined in vitro against HEK293 and hRBC. The compounds were non-hemolytic at their active concentrations, i.e., they did not lysis 10% of hRBCs at their MIC_{80} values. However, well-defined, or partial cytotoxicity was observed for some compounds. For instance, although compound **9q** bears a considerably safe margin as an anticryptococcal agent (MIC_{80} = 12.57 µM), its anticandidal potential (MIC_{80} = 25.13 µM) is compromised by a CC_{50} value of 26.58 µM, lower than tamoxifen (CC_{50} = 35.15 µM) used as the reference toxin. Compounds **9d**, **10c**, **10d**, **10j**, and **10z** also share a similar fate with **9q**, albeit with reduced

Table 1 Antimicrobial potentials of quinoline—1*H*-1,2,3-triazole hybrids

Compound	Structure	Antimicrobial activity MIC_{80} (μM)							Cytotoxicity (μM)	
		Gram +ve	Gram –ve				Fungi		CC_{50}	HC_{10}
		MRSA	*E. c.*	MDR *K. p.*	*P. a.*	*A. b.*	*C. a.*	*C. n.*		
8-HQ	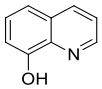	55.11	–	–	–	220.45	13.78	3.44	–[a]	–
9d	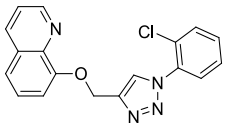	–	–	–	–	–	95.02	47.51	67.70	–
9 *l*	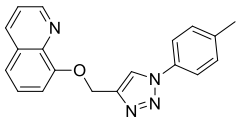	–	–	–	–	79.6%*	–	101.15	–[a]	–
9q	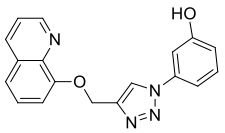	–	–	–	–	–	25.13	12.57	26.58	–
9r	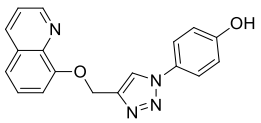	–	–	–	–	–	100.52	50.26	–[a]	–
10a	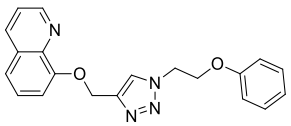	–	–	–	–	–	92.38	46.19	–[a]	–
10c	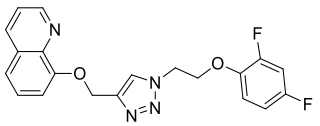	–	–	–	–	–	83.69	41.85	68.00	–
10d	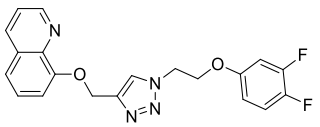	–	–	–	–	–	83.69	20.92	66.95	–
10e	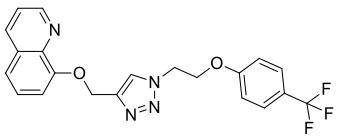	–	–	–	–	–	77.22	38.61	–[a]	–
10j	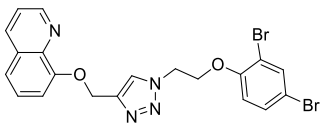	–	–	–	–	–	63.47	31.74	54.55	–
10m	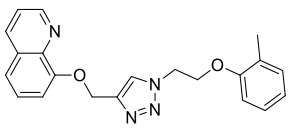	–	–	–	–	–	88.79	88.79	–	–
10n	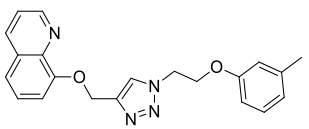	–	–	–	–	–	88.79	44.39	–	–

Table 1 (continued)

Compound	Structure	Antimicrobial activity MIC_{80} (μM)							Cytotoxicity (μM)	
		Gram +ve	Gram –ve				Fungi		CC_{50}	HC_{10}
		MRSA	*E. c.*	MDR *K. p.*	*P. a.*	*A. b.*	*C. a.*	*C. n.*		
10q	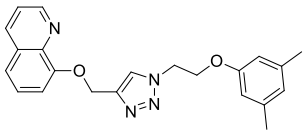	–	–	–	–	–	85.46	–	–	–
10l	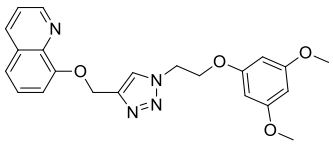	–	–	–	–	–	78.73	–	–	–
10v	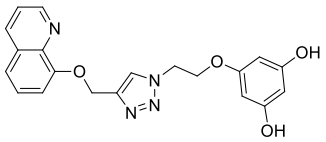	84.57	–	–	–	–	42.29	21.14	–[a]	–
10z	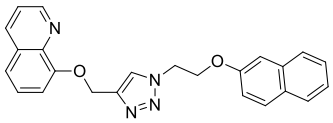	–	–	–	–	–	80.72	20.18	42.88	–
11a	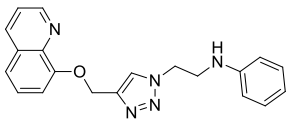	–	–	–	–	–	92.65	46.32	–[a]	–
11d	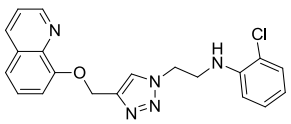	–	–	–	–	–	84.25	42.12	–	–
14	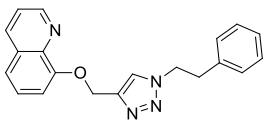	–	–	–	–	–	–	–	nd	nd
15	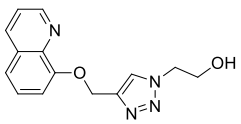	–	–	–	–	–	–	–	nd	nd
16	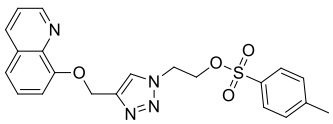	75.39	75.39	75.39	64.8%*	75.39	37.69	2.36	–[a]	–
17	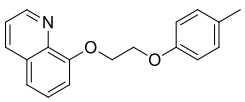	–	–	–	–	–	–	–	nd	nd
18	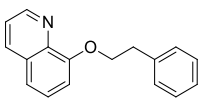	128.35	–	–	–	128.35	32.09	16.04	–[a]	–
19**	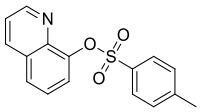	nd	–[c]	–[c]	–[c]	nd	nd	nd	nd	nd

Table 1 (continued)

Compound	Structure	Antimicrobial activity MIC_{80} (μM)							Cytotoxicity (μM)	
		Gram +ve	Gram –ve				Fungi		CC_{50}	HC_{10}
		MRSA	*E. c.*	MDR *K. p.*	*P. a.*	*A. b.*	*C. a.*	*C. n.*		
Colistin-Sulfate		–	0.09	0.18	0.18	0.18				
Vancomycin-HCl		0.67	–	–	–	–				
Fluconazole							0.41	26.12		
Tamoxifen									35.15	
Melittin										0.17

MIC_{80}: minimum concentration inhibiting ≥ 80% growth of microbial cell; CC_{50}: concentration at 50% cytotoxicity to HEK293; HC_{10}: concentration at 10% hemolytic activity against hRBCs; MRSA: methicillin-resistant *Staphylococcus aureus*; *E. c.*: *Escherichia coli*; MDR *K. p.*: multidrug-resistant *Klebsiella pneumoniae*; *P. a.*: *Pseudomonas aeruginosa*; *A. b.*: *Acinetobacter baumannii*; *C. a.*: *Candida albicans*; *C. n.*: *Cryptococcus neoformans*; '–': inactive at maximum tested concentration of 32 μg/mL; *: percentage growth inhibition at 32 μg/mL; '–[a]': compounds showing partial toxicity at 32 μg/mL in a replicate but inactive in the other; **: values from Aneja et al. 2018. '–[c]': $IC_{50} > 400$ μM

cytotoxicity compared to tamoxifen. Furthermore, the most potent compound **16** showed partial cytotoxicity with $CC_{50} = 68.56$ μM akin to compounds **9*l***, **9r**, **10a**, **10e**, **10v**, **11a,** and **18**. In contrast, compounds **10 m**, **10n**, **10q**, **10*l***, and **11d** were non-cytotoxic at their MIC_{80} values. Therefore, further structural optimization of these hybrids, especially compound **16**, is pertinent.

In silico studies

ADME properties

Absorption, distribution, metabolism, and excretion (ADME) are fundamental pharmacokinetic properties useful for evaluation of the drugability of promising drug candidates as well as early identification of compounds that are likely to fail clinical trials. Their evaluation through in silico predictions also helps to fast-track the drug development process while reducing cost. Thus, the ADME properties of active hybrids in this study were computed with QikProp 6.0 [28] implemented in the Schrödinger molecular modeling suite (version 2019-2).

The worthiness of compound **16** for further structural optimization is supported by its excellent drug-like properties (Table 2), adjudged by the zero-violation of Lipinski's rule of five (Ro5) and Jorgensen's rule of three (Ro3). Precisely, high oral absorption is obtainable considering the apposite balance of corresponding descriptors, i.e., molecular weight (MW), hydrogen bonding donor/acceptor (HBD/A), predicted total solvent accessible surface area (SASA), aqueous solubility (QPlogS), and lipophilicity ($QPlogP_{o/w}$). Favorable plasma distribution (bioavailability) for adequate exposure to therapeutic targets is also expected, considering the mid-ranged binding affinity to human serum albumin (QPlogKhsa) [27, 29]. The predicted potential blockage of hERG K^+ ion channel (QPlogHERG) for QT prolongation and torsades de pointes (TdP) arrhythmia should be interpreted with caution, as not all hERG blockers pose a pro-TdP arrhythmic risk [30]. Albeit, further optimization studies should seek to reduce this property. The predicted sites of metabolism of examined hybrids, together with the ADME properties of other active hybrids, are given in the Online Resource (Fig. S1 and Table S1, respectively).

Binding interactions with drug targets

In order to rationalize the observed antimicrobial activities, potent hybrids were docked into the active sites of antibacterial drug target: phospho-MurNAc-pentapeptide

Table 2 Predicted ADME properties of compound 16

	MW	SASA	HBD	HBA	QPlogPo/w	QPlogS	QPlogHERG	QPlogKhsa	Oral abs	Ro5	Ro3
Compound 16	424.47	780.47	0	8	3.54	−5.39	−7.61	−0.04	95%	0	0
Acceptable range	130.0–725.0	300.0–1000.0	0–6	2–20	−2.0 to 6.5	−6.5 to 0.5	> −5	–1.5 to 1.5	> 80%	< 4	< 3

MW: molecular weight; SASA: total solvent accessible surface area in $Å^2$; HBD: hydrogen bond donor; HBA: hydrogen bond acceptor; QPlogPo/w: octanol/water partition coefficient; QPlogS: aqueous solubility S in mol dm^{-3}; QPlogHERG: IC_{50} value for the blockage of "human ether-*a-go-go* related gene" K^+ channels; QPlogKhSA: binding to human serum albumin; Oral abs: human oral absorption; Ro5: Lipinski's rule of five; Ro3: Jorgensen's rule of three

translocase (MraY) [31], and antifungal drug target: lanosterol 14α-demethylase (LDM) [32].

MraY

The molecular modeling of compound **16** in the cytoplasmic active site of MraY (PDB ID: 4J72) revealed that the ligand accesses the receptor's active site-cleft via the quinoline fragment. The 8-*O* atom thus coordinates catalytically essential Mg^{2+} cofactor in the binding site, while the pyridine *N*-atom is favorable to interact in like manner (Fig. 3a). Subsequently, the triazole H-5' atom forms an aromatic H-b with Asp117 and Asp265 of the catalytic aspartic acid triad residues, while the quinoline benzene ring is involved in pi-pi stacking interaction with highly conserved His324 of the HHH motif. The oxygen atoms of the tosylate unit also afforded H-b interaction with side-chain amino units of Gln137, Lys133, and Asn190. Aromatic H-b interaction of the tosyl ring with Gln137 and Asp193 as well as hydrophobic contacts with Phe134, Phe262, and Met263 stabilized the ligand–receptor complex. These interactions induced critical conformational changes in the protein structure, as evidenced by the coordination of Asn190, Asp193, and Gly264 to Mg^{2+} cofactor to foster a tight receptor binding (Table 3).

Furthermore, the similar binding modes of compound **10v** (Fig. 3b), particularly H-b interactions with the catalytic aspartic acid triad (Asp117, Asp118, and Asp265) and pi-cation interaction with catalytic Mg^{2+} ion, support its activity against MRSA. However, the single-spectrum

Table 3 Molecular docking results of compound 16 and other potent hybrids at the cytoplasmic active site of MraY

Compound	Docking score	Glide gscore	Glide emodel	Glide energy
16	−7.56	−7.56	−70.12	−49.13
10v	−4.99	−7.51	−72.48	−58.15
8-HQ	−3.83	−5.91	−21.66	−16.18
19	−3.86	−3.86	−44.36	−38.59

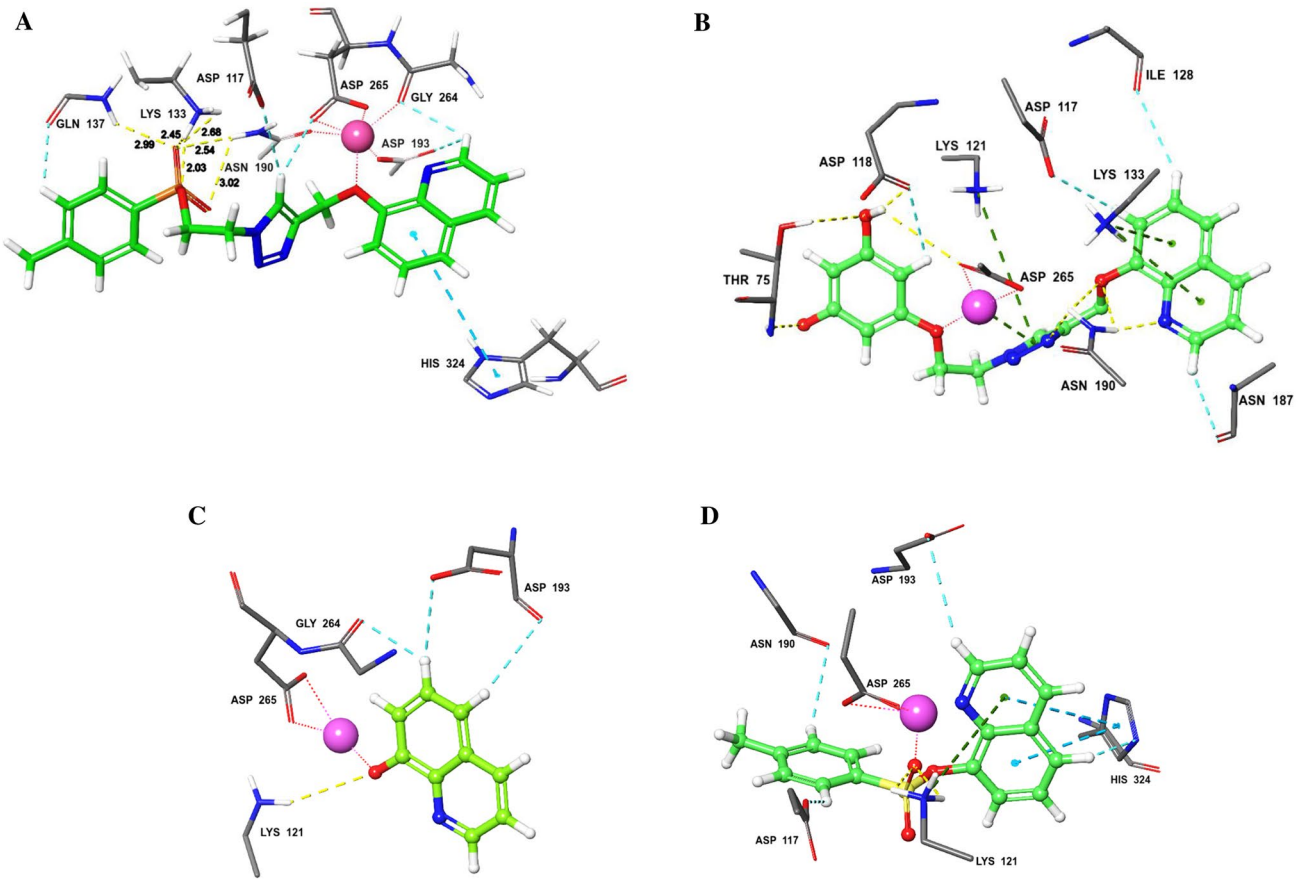

Fig. 3 Predicted binding modes of compound 16 (**a**), 10v (**b**), 8-HQ (**c**) and 19 (**d**) in the cytoplasmic active site of MraY. Protein interactions are displayed as dashed lines; hydrogen bond (yellow), aromatic H-bond (cyan), pi-pi stacking (light-blue) pi-cation (green) and metal-coordination (red). Atoms: carbon (ligand: green; protein: gray), nitrogen (blue), oxygen (red), sulfur (yellow), hydrogen (white), Mg^{2+} cofactor (purple sphere)

antibacterial activity can be partly justified by the ligand's loose binding at the receptor's active site, lack of interaction with His324, and the inability to induce increased coordination to Mg^{2+} ion. Similar rationalizations and the absence of the 1*H*-1,2,3-triazole ring are valid for the activity profile of **8-HQ** and compound **19** (Fig. 3c, d, respectively).

LDM

The binding profiles of compounds **9q**, **10d**, **10v**, **10z**, **16**, **18,** and their precursor **8-HQ** were simulated at the heme-containing active site of LDM (PDB ID: 4WMZ). Analysis of compound **16**-LDM complex (Fig. 4) showed that the 1*H*-1,2,3-triazole ring is crucial to strong protein binding. The ring assumed a conformation identical to the 1,2,4-triazole unit of fluconazole near the heme cofactor, thus affording compound **16** the best binding profile overall (Table 4). The docked complex features pi-pi stacking and pi-cation interactions of the 1*H*-1,2,3-triazole with porphyrin ring and Fe^{3+} ion of heme cofactor, respectively, while the H-5' atom forms an aromatic H-b interaction with Tyr140. Also, the sulfone unit presented H-b and aromatic H-b interactions with Gly314 and Tyr140, respectively; the quinoline ring interacted in like manner with Tyr126 and Ser382. The predicted binding modes of other hybrids (Table 4) corroborate their antifungal activities.

Conclusion

A library of quinoline–1*H*-1,2,3-triazole molecular hybrids was developed as antimicrobial agents using CuAAC. Compound **16** was established as a promising scaffold with a broad-spectrum antimicrobial activity against the examined pathogens. SAR analysis and molecular docking studies established the significance of molecular hybridization to antimicrobial activity as each pharmacophore on the hybrid concertedly contributed to the observed antimicrobial profile. These results suggest that further structural optimization of the identified compound is relevant to afford new antimicrobial agents with stronger potencies.

Experimental

General information

All reagents were used as purchased from Merck through Capital Laboratory, South Africa. The progress of all reactions was monitored with thin-layer chromatography (TLC) on Merck alumina-backed TLC plates and visualized under UV light. Product purification was achieved using column chromatography with silica gel (0.063–0.200 mm) and appropriate ratios of hexane–EtOAc or EtOAc-methanol as eluant. Infrared (IR) spectra were recorded on a PerkinElmer 100 spectrophotometer with Universal ATR sampling accessory; wavenumbers (υ) are expressed in cm^{-1}. NMR spectra were obtained from Bruker Avance ^{III} 400 or 600 Hz spectrometers at 400 or 600 Hz for ^{1}H and 101 or 151 for ^{13}C. Chemical shifts (δ) are reported in parts per million (ppm) relative to tetramethylsilane (TMS) as internal standard, and the coupling constants (*J*) are reported in Hertz (Hz). Splitting patterns are denoted as follows: singlet (s), doublet (d), multiplet (m), triplet (t), quartet (q), doublet of doublets (dd), doublet of triplets (dt), triplet of doublets (td), and doublet of quartet (dq). Phenyl ring is denoted as "Ph," while quaternary carbons are distinguished with a "q." The exact molecular mass of target hybrids was obtained from Waters Micromass LCT Premier TOF–MS spectrometer. Melting points were determined with Stuart melting point instrument

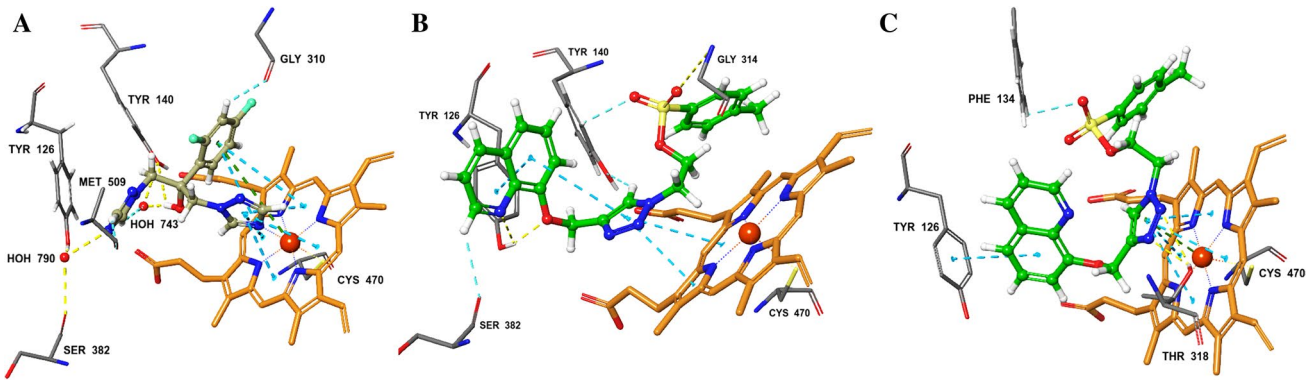

Fig. 4 Binding modes of fluconazole and compound 16 around heme cofactor in the active site of LDM. **a** Fluconazole. **b** Compound 16 Pose 1. **c** Pose 2. Protein interactions are displayed as dashed lines; hydrogen bond (yellow), aromatic H-bond (cyan), pi-pi stacking (light-blue) pi-cation (green) and metal-coordination (red). Atoms: nitrogen (blue), oxygen (red), fluorine (lime green), carbon-compound 16 (green); fluconazole (beige); protein (gray); heme cofactor (brown tubes). Fe^{3+} ion (brown sphere). Water (red balls)

Table 4 Molecular docking results and binding modes of potent hybrids ($MIC_{80} < 26$ μM) at the active site of LDM

Compound	Docking score	Glide gscore	Glide emodel	Glide energy	Key binding interactions			pi-cation (Fe^{3+})
					Hydrogen bonding (H-b)	aromatic H-b	pi-pi stacking	
8-HQ	− 7.76	− 7.78	− 32.51	− 25.68	Tyr126 (8-OH, N-1), Ser382 (8-OH)	None	Tyr126 (quinoline)	None
9q	− 10.44	− 10.45	− 83.15	− 52.29	Gly310, Val311, Gly314, Gly315 (*m*-OH phenyl), Tyr126 (8-*O*, *N*-1 quinoline)	Tyr140 (H-5 triazole), Ser382 (H-2 quinoline)	Heme (phenyl, triazole), Phe384, Tyr126 (quinoline)	Phenyl
10d	− 9.81	− 9.81	− 89.23	− 50.93	None	Leu129 (H-2 quinoline), Tyr140 (H-5 triazole), Gly310 (H-5 phenoxy)	Heme (triazole, phenoxy), Tyr126 (triazole), Phe236 (quinoline)	Phenoxy
10v	− 9.80	− 9.81	− 106.30	− 63.26	Tyr126 (*O*-1 phenoxy), Pro379, His381, Ser382, Met509 (3-OH phenoxy), Phe506, Thr507, Ser508 (5-OH phenoxy)	Tyr140 (H-2 phenoxy), His381 (3-OH phenoxy), Ser508 (H-4 phenoxy)	Heme (quinoline), Tyr126 (triazole), His381 (phenoxy)	Quinoline
10z	− 11.07	− 11.08	− 104.57	− 56.65	Tyr126 (*O*-2 naphthoxy, *N*-2 triazole)	H-4 quinoline (Gly310, Val311), Leu129 (H-6, H-7 naphthoxy), Thr237 (H-5, H-6 naphthoxy)	Heme (quinoline, triazole), Phe236 (naphthoxy)	Quinoline
16	− 12.04	− 12.04	− 107.87	− 62.69	Tyr126 (8-*O*, *N*-1 quinoline), Gly314 (SO_2)	Tyr140 (H-5 triazole; SO_2), Ser382 (H-2 quinoline)	Heme (triazole), Tyr126 (quinoline)	Triazole
18	− 9.11	− 9.11	− 51.22	− 36.87	Tyr126 (*O*-8, *N*-1 quinoline)	Tyr140 (H-2 phenyl), Ser382 (H-2 quinoline)	Heme (phenyl), Tyr126 (quinoline)	none

(SMP-3) in open-end capillary tubes and were uncorrected. The general synthetic procedures for azide precursors, compounds **17** and **18**, are given in Online Resource.

Preparation of 8-(prop-2-yn-1-yloxy)quinoline (8)

5.89 g (40.58 mmol, 1 eq.) of **8-HQ** was added to a stirring solution of anhydrous potassium carbonate (6.91 g, 50 mmol, 1.23 eq.) in 40 mL DMF at room temperature (RT). After few minutes, the solution turned yellow, and then, 3.62 mL (42 mmol, 1.04 eq.) of propargyl bromide (80% in toluene) in DMF (5 mL) was added and stirring continued at RT for 4 h. After that, the reaction mixture was poured into a slurry of ice, stirred, and filtered *in vacuo* to afford 6.90 g of deep brown solid.

Chemical formula: $C_{12}H_9NO$; Yield: 93%; Mol. wt: 183.21 g/mol; $R_f = 0.51$ (EtOAc-hexane 80:20). mp: 66–68 °C.

FT-IR: 3275 (C≡C–H), 2121 (C≡C), 1501 (C=N), 1266 (C–O–C) cm^{-1}.

^{1}H NMR (400 MHz, Chloroform-*d*) δ 8.94 (dd, *J* = 4.2, 1.7 Hz, 1H, C*H*-2), 8.13 (dd, *J* = 8.3, 1.7 Hz, 1H, C*H*-4), 7.53–7.39 (m, 3H, C*H*-6,5,3), 7.26 (dd, *J* = 7.2, 1.7 Hz, 1H, C*H*-7), 5.03 (d, *J* = 2.4 Hz, 2H, OCH_2-9), 2.54 (t, *J* = 2.4 Hz, 1H, C*H*-11).

^{13}C NMR (101 MHz, Chloroform-*d*) δ 153.09 (*C*q-8), 149.45 (*C*-2), 140.34 (*C*q-8a), 135.95 (*C*-4), 129.49 (*C*q-4a), 126.43 (*C*-6), 121.73 (*C*-3), 120.66 (*C*-5), 109.96 (*C*-7), 78.30 (*C*q-10-), 76.08 (*C*-11), 56.52 (O-*C*-9).

General synthetic procedure for quinoline-1*H*-1,2,3-triazole molecular hybrids

To a 15 mL DCM solution of *O*-propargylated quinoline **8** (0.2 g, 1.09 mmol, 1 eq.) in a round-bottom flask (100 mL), appropriate azide (1 eq.) was dissolved, then a solution of 10 mol% $CuSO_4.5H_2O$ and 22 mol% sodium ascorbate in water (15 mL) was added, and the flask's contents were stirred at RT for 2–4 h. After the reaction was complete, as evident by the consumption of alkyne (**8**) on TLC, the reaction mixture was diluted with water, filtered, and extracted with DCM. Then, the combined DCM extracts were dried over anhydrous sodium sulfate, filtered, and concentrated *in vacuo*. Finally, the target hybrids were obtained in good yields after column chromatography using hexane–EtOAc or EtOAc–MeOH as eluant. The spectral data of active hybrids shown in Table 1 are given below, while those of other compounds along with the FT-IR, NMR, and HRMS spectra of all compounds are presented in the Online Resource.

8-((1-(2-chlorophenyl)-1H-1,2,3-triazol-4-yl)methoxy) quinoline (9d) Dark brown solid; Yield: 73%; Chemical formula: $C_{18}H_{13}ClN_4O$; Mol. wt: 336.78 g/mol; R_f: 0.42 (EtOAc-hexane 80:20); mp: 112–114 °C.

FT-IR: 3057 (C-H_{Ar}), 2875 (OCH_2), 1497 (C=N), 1102 (C_{Ar}–Cl) cm^{-1}.

^{1}H NMR: (400 MHz, Chloroform-*d*) δ 8.96 (s, 1H, C*H*-2), 8.24 (s, 1H, C*H*-5' triazole), 8.18 (d, *J* = 8.2 Hz, 1H, C*H*-4), 7.65–7.59 (m, 1H, C*H*-9'), 7.59–7.54 (m, 1H, C*H*-12'), 7.53–7.48 (m, 1H, C*H*-6), 7.48–7.37 (m, 5H, C*H*-3,5,7,10',11'), 5.70 (s, 2H, OCH_2-6').

^{13}C NMR: (101 MHz, Chloroform-*d*) δ 153.83 (*C*-8), 149.36 (*C*–2), 143.86 (*C*-4' triazole), 140.33 (*C*-8a), 136.01 (*C*-4), 134.80 (*C*-7'), 130.80, (10') 130.73 (12'), 129.51 (*C*-4a), 128.66 (*C*-8'), 127.88 (*C*-11'), 127.77 (*C*-9'), 126.70 (*C*-6), 125.47 (*C*-5' triazole), 121.66 (*C*-3), 120.41 (*C*-5), 110.16 (*C*-7), 62.87 (O*C*H_2-6').

HRMS: (ESI$^+$-MS, *m/z*) calcd for $C_{18}H_{13}ClN_4O$ $(M+Na)^+$: 359.0676, found: 359.0684.

8-((1-(p-tolyl)-1H-1,2,3-triazol-4-yl)methoxy)quinoline(9 l) Brown solid; Yield: 66%; Chemical formula: $C_{19}H_{16}N_4O$; Mol. wt: 316.36 g/mol; R_f : 0.43 (EtOAc-hexane 80:20); mp: 126–128 °C.

FT-IR: 3078 (C-H_{Ar}), 2920 (Ar–CH_3), 1496 (C=N) cm^{-1}.

^{1}H NMR: (400 MHz, Chloroform-*d*) δ 8.95 (dd, 4.3, 1.6 Hz, 1H, C*H*-2), 8.16 (s, 1H, C*H*-5' triazole), 8.13 (dd, *J* = 8.3, 1.6 Hz, 1H, C*H*-4), 7.58 (d, *J* = 8.2 Hz, 2H, C*H*-9',11'), 7.49–7.38 (m, 3H, C*H*-6,5,3), 7.36 (dd, *J* = 7.3, 1.5 Hz, 1H, C*H*-7), 7.28 (d, *J* = 8.2 Hz, 2H, C*H*-8',12'), 5.64 (s, 2H, OCH_2-6'), 2.39 (s, 3H Ar-CH_3-13').

^{13}C NMR: (101 MHz, Chloroform-*d*) δ 153.83 (*C*q-8), 149.38 (*C*-2), 144.65 (*Cq*-4' triazole), 140.33 (*C*q-8a), 138.91 (*C*q-7'), 135.98 (*C*-4), 134.68 (*C*q-4a), 130.20 (*C*-8',12'), 129.51 (*C*q-10'), 126.73 (*C*-6), 121.66 (*C*-3), 121.48 (*C*-5' triazole), 120.46 (*C*-9',11'), 120.30 (*C*-5'), 109.93 (*C*-7), 62.88 (O-*C*-6'), 21.07 (Ar-*C*-13').

HRMS: (ESI$^+$-MS, *m/z*) calcd for $C_{19}H_{16}N_4O$ $(M+Na)^+$: 339.1222, found: 339.1212.

3-(4-((quinolin-8-yloxy)methyl)-1H-1,2,3-triazol-1-yl) phenol (9q) Brown solid; Yield: 62%; Chemical formula: $C_{18}H_{14}N_4O_2$; Mol. wt: 318.33 g/mol; R_f: 0.27 (EtOAC-Hexane 80:20); mp: 248–249 °C.

^{1}H NMR (400 MHz, DMSO-d_6): δ 10.07 (s, 1H, O*H*-13'), 8.96 (s, 1H, C*H*-5' triazole), 8.83 (d, *J* = 3.8 Hz, 1H, C*H*-2), 8.32 (dd, *J* = 8.3, 1.7 Hz, 1H, C*H*-4), 7.58–7.50 (m, 3H, C*H*-6,5,3), 7.45 (dd, *J* = 5.7, 3.3 Hz, 1H, C*H*-7), 7.39 (t, *J* = 8.3 Hz, 1H, C*H*-11'), 7.35–7.29 (m, 2H, C*H*-8',10'), 6.89 (dd, 1H, C*H*-12'), 5.43 (s, 2H, OCH_2-6').

^{13}C NMR (101 MHz, DMSO-d_6): δ 158.45 (*C*q-9'), 153.76 (*C*q-8), 148.98 (*C*-2), 143.55 (*C*q-4' triazole), 139.71 (*C*q-8a), 137.52 (*C*q-7'), 135.79 (*C*-4), 130.76 (*C*-11'), 129.06 (*C*q-4a), 126.72 (*C*-6), 123.17 (*C*-5' triazole),

121.87 (*C*-3), 120.16 (*C*-5), 115.70 (*C*-12'), 110.50 (*C*-10'), 110.17 (*C*-7), 107.06 (*C*-8'), 61.67 (O-*C*-6').

HRMS: (ESI$^+$-MS, *m/z*) calcd for $C_{18}H_{14}N_4O_2$ $(M+Na)^+$: 341.1014, found: 341.1008.

4-(4-((quinolin-8-yloxy)methyl)-1H-1,2,3-triazol-1-yl) phenol (9r) Brown solid; Yield: 44%; Chemical formula: $C_{18}H_{14}N_4O_2$; Mol wt: 318.33 g/mol; R_f: 0.36 (EtOAC-Hexane 80:20); mp: 277–279 °C.

^{13}H NMR (400 MHz, DMSO-d_6): δ 9.95 (s, 1H, O*H*-13'), 8.91–8.76 (m, 2H, C*H*-5' triazole, C*H*-2), 8.32 (dd, *J* = 8.3, 1.7 Hz, 1H, C*H*-4), 7.69 (dd, *J* = 8.8 Hz, 2H, C*H*-8',12'), 7.63–7.50 (m, 3H, C*H*-6,5,3), 7.45 (dd, *J* = 5.5, 3.5 Hz, 1H, C*H*-7), 6.94 (dd, *J* = 8.8 Hz, 2H, C*H*-9',11'), 5.42 (s, 2H, OCH_2-6').

^{13}C NMR (101 MHz, DMSO-d_6): δ 157.78 (*C*q-10'), 153.79 (*C*q-8), 148.96 (*C*-2), 143.30 (*C*q-4' triazole), 139.71 *C*q-8a), 135.78 (*C*-4), 129.05 (*C*q-4a), 128.69 (*C*q-7'), 126.73 (*C*-6), 123.09 (*C*-5' triazole), 122.03, 121.85 (*C*-3), 120.11 (*C*-5), 116.02 (*C*-9',11'), 110.12 (*C*-7), 61.75 (O-*C*-6').

HRMS: (ESI$^+$-MS, *m/z*) calcd for $C_{18}H_{14}N_4O_2$ $(M+Na)^+$: 341.1014, found: 341.1008.

8-((1-(2-phenoxyethyl)-1H-1,2,3-triazol-4-yl)methoxy) quinoline (10a) Light brown solid; Yield: 59%; Chemical formula: $C_{20}H_{18}N_4O_2$; Mol. wt: 346.38 g/mol; R_f: 0.20 (EtOAc-hexane 80:20); mp: 108–110 °C.

^{1}H NMR (400 MHz, Chloroform-*d*): δ 8.94 (s, 1H, C*H*-2), 8.16 (s, 1H, C*H*-4), 7.98 (s, 1H, C*H*-5'triazole), 7.41 (s, 1H, C*H*-6), 7.35 (s, 3H, C*H*-5,3,7), 7.27–7.20 (t, *J* = 7.8 Hz, 2H, C*H*-3'',5''), 6.95 (t, *J* = 7.4 Hz, 1H, C*H*-4''), 6.81–6.79 (d, *J* = 7.8 Hz, 2H, C*H*-2'',6''), 5.60 (s, 2H, O-CH_2-6'), 4.72 (t, *J* = 5.0 Hz, 2H, N–CH_2-7'), 4.33 (t, *J* = 5.0 Hz, 2H, O-CH_2-8').

^{13}C NMR (101 MHz, Chloroform-*d*): δ 157.69 (O-*C*q-1"), 153.29 (*C*-2), 144.22 (*C*q-4' triazole), 129.59 (*C*-3",5"), 126.88 (*C*-6), 124.48 (*C*-5' triazole), 121.65 (*C*-4"), 114.52 (*C*-2",6"), 110.49 (*C*-7), 66.12 (O-*C*-8'), 62.83 (O-*C*-6'), 49.81 (N–*C*-7'). Not observed (*C*-3,4,5,8,8a,4a).

HRMS: (ESI$^+$-MS, *m/z*) calcd for $C_{20}H_{18}N_4O_2$ $(M+Na)^+$: 369.1335, found: 369.1327.

8-((1-(2-(2,4-difluorophenoxy)ethyl)-1H-1,2,3-triazol-4-yl)methoxy)quinoline (10c) Cream solid; Yield: 52%; Chemical formula: $C_{20}H_{16}F_2N_4O_2$; Mol. wt: 382.36 g/mol; R_f: 0.15 (EtOAc-hexane 80:20); mp: 136–138 °C.

^{1}H NMR (600 MHz, Chloroform-*d*): δ 8.93 (s, 1H, C*H*-2), 8.14 (s, 1H, C*H*-4), 7.98 (s, 1H, C*H*-5'triazole), 7.50–7.30 (m, 4H, C*H*-6,5,3,7), 6.81–6.72 (m, 2H, C*H*-5'',3''), 6.68 (dddd, *J* = 9.2, 7.8, 3.0, 1.6 Hz, 1H, C*H*-6''), 5.60 (s, 2H, O-CH_2-6'), 4.72 (t, *J* = 5.0 Hz, 2H, N–CH_2-7'), 4.35 (t, *J* = 5.0 Hz, 2H, O-CH_2-8').

^{13}C NMR (151 MHz, Chloroform-*d*): δ 157.26 (dd, *J* = 243.5, 10.4 Hz, *C*q-2''), 152.80 (dd, *J* = 249.8, 12.1 Hz, *C*q-4''), 144.32 (*C*q-4' triazole), 142.36 (dd, *J* = 10.9, 3.6 Hz, *C*q-1''), 135.86 (*C*-4), 126.79 (*C*-6), 124.62 (*C*-5' triazole), 121.58 (*C*-3), 120.28 (*C*-5), 117.04 (d, *J* = 8.5 Hz, *C*-6''), 110.63 (dd, *J* = 22.6, 3.9 Hz, *C*-5''), 110.07 (*C*-7), 105.07 (dd, *J* = 26.8, 22.2 Hz, *C*-3''), 69.02 (O-*C*-8'), 62.85 (O-*C*-6'), 49.86 (N–*C*-7'). Not observed (*C*-2,8,8a,4a).

8-((1-(2-(3,4-difluorophenoxy)ethyl)-1H-1,2,3-triazol-4-yl)methoxy)quinoline (10d) Cream solid; Yield: 54%; Chemical formula: $C_{20}H_{16}F_2N_4O_2$; Mol. wt: 382.36 g/mol; R_f: 0.15 (EtOAc-hexane 80:20); mp: 110–112 °C.

^{1}H NMR (400 MHz, Chloroform-*d*): δ 8.95 (s, 1H, C*H*-2), 8.17 (s, 1H, C*H*-4), 7.94 (s, 1H, C*H*-5' triazole), 7.63–7.17 (m, 4H, C*H*-6,5,3,7), 7.00 (q, *J* = 9.3 Hz, 1H, C*H*-5''), 6.60 (ddd, *J* = 11.7, 6.5, 2.9 Hz, 1H,, C*H*-2''), 6.47 (dq, *J* = 8.5, 2.7 Hz, 1H,, C*H*-6''), 5.60 (s, 2H, O-CH_2-6'), 4.72 (t, *J* = 5.0 Hz, 2H, N–CH_2-7'), 4.29 (t, *J* = 5.0 Hz, 2H, O-CH_2-8').

^{13}C NMR (101 MHz, Chloroform-*d*): δ 153.94 (dd, *J* = 8.5, 2.3 Hz, *C*q-1''), 150.39 (dd, *J* = 248.6, 13.9 Hz, *C*q-3''), 145.50 (dd, *J* = 242.9, 11.3 Hz, *C*q-4''), 144.37 (*C*q-4' triazole), 126.81 (*C*-6), 124.40 (*C*-5' triazole), 117.33 (dd, *J* = 18.6, 1.4 Hz, (*C*-5''), 109.72 (dd, *J* = 5.8, 3.5 Hz, *C*-7,6''), 104.50 (d, *J* = 20.4 Hz, *C*-2''), 66.97 (O-*C*-8'), 62.79 (O-*C*-6'), 49.60 (N–*C*-7'). Not observed (*C*-2,3,4,5,8,8a,4a).

HRMS: (ESI$^+$-MS, *m/z*) calcd for $C_{20}H_{16}F_2N_4O_2$ $(M+Na)^+$: 405.1139, found: 405.1149.

8-((1-(2-(4-(trifluoromethyl)phenoxy)ethyl)-1H-1,2,3-triazol-4-yl)methoxy)quinoline (10e) Dark brown crystalline solid; Yield: 37%; Chemical formula: $C_{21}H_{17}F_3N_4O_2$; Mol. wt: 414.38 g/mol; R_f: 0.17 (EtOAc-hexane 80:20); mp: 150–152 °C.

^{1}H NMR (600 MHz, Chloroform-*d*): δ 8.93 (s, 1H, C*H*-2), 8.12 (d, *J* = 8.2 Hz, 1H, C*H*-4), 7.92 (s, 1H, C*H*-5' triazole), 7.48 (d, *J* = 8.4 Hz, 2H, C*H*-3'',5''), 7.44–7.38 (m, 3H, C*H*-6,5,3), 7.30 (d, *J* = 6.7 Hz, 1H, C*H*-7), 6.84 (d, *J* = 8.4 Hz, 2H, C*H*-2'',6''), 5.58 (s, 2H, O-CH_2-6'), 4.74 (t, *J* = 5.1 Hz, 2H, N–CH_2-7'), 4.38 (t, *J* = 5.1 Hz, 2H, O-CH_2-8').

^{13}C NMR (151 MHz, Chloroform-*d*): δ 160.12 (*C*q-1''), 153.82 (*C*q-8), 149.35 (*C*-2), 144.42 (*C*q-4' triazole), 140.40 (*C*q-8a), 135.94 (*C*-4), 129.52 (*C*q-4a), 127.02 (q, *J* = 3.8 Hz, *C*-3'',5''), 126.69 (*C*-6), 124.37 (*C*-5' triazole), 125.44–122.80 (m, Ph-*C*q-7''), 121.64 (*C*-3), 120.25 (*C*-5), 114.51 (*C*q-2'',6''), 110.02 (*C*-7), 66.40 (O-*C*-8'), 62.87 (O-*C*-6'), 49.56 (N–*C*-7').

HRMS: (ESI$^+$-MS, *m/z*) calcd for $C_{21}H_{17}F_3N_4O_2$ $(M+Na)^+$: 437.1201, found: 437.1211

8-((1-(2-(2,4-dibromophenoxy)ethyl)-1H-1,2,3-triazol-4-yl)methoxy)quinoline (10j) Brown solid; Yield: 88%; Chemical formula: $C_{20}H_{16}Br_2N_4O_2$; Mol. wt: 504.17 g/mol; R_f: 0.26 (EtOAc-Hexane, 80:20); mp: 129–131 °C.

^{1}H NMR (600 MHz, Chloroform-*d*): δ 8.92 (s, 1H, C*H*-2), 8.18–8.08 (m, 1H, C*H*-4), 8.04 (s, 1H, C*H*-5' triazole), 7.56–7.51 (m, 2H, C*H*-5'',3''), 7.49–7.21 (m, 5H, C*H*-6,5,3,7,6''), 5.62 (s, 2H, O-CH_2-6'), 4.77 (t, *J* = 4.9 Hz, 2H, N–CH_2-7'), 4.28 (t, *J* = 4.9 Hz, 2H, O-CH_2-8').

^{13}C NMR (151 MHz, Chloroform-*d*): δ 153.53 (*C*q-8), 151.46 (*C*q-1''), 144.23 (*C*q-4' triazole), 135.63 (*C*-4), 135.05 (*C*-3'',5''), 131.24 (*C*-6''), 126.75 (*C*-6), 124.97 (*C*-5' triazole), 121.85 (*C*-3), 120.37 (*C*-5), 118.71 (*C*q-2''), 118.21 (*C*q-4''), 110.00 (*C*-7), 70.70 (O-*C*-8'), 62.85 (O-*C*-6'), 50.20 (N–*C*-7'). Not observed (*C*-2,8a,4a).

HRMS: (ESI$^+$-MS, *m/z*) calcd for $C_{20}H_{16}Br_2N_4O_2$ $(M+Na)^+$: 524.9538, found: 524.9545.

8-((1-(2-(3,5-dimethoxyphenoxy)ethyl)-1H-1,2,3-triazol-4-yl)methoxy)quinoline (10l) Beige solid; Yield: 69%; Chemical formula: $C_{22}H_{22}N_4O_4$; Mol. wt: 406.43 g/mol; R_f: 0.17 (EtOAc-Hexane, 80:20); mp: 138–140 °C.

^{1}H NMR (600 MHz, Chloroform-*d*): δ 8.95 (s, 1H, C*H*-2), 8.14 (s, 1H, C*H*-4), 7.96 (s, 1H, C*H*-5' triazole), 7.41–7.45 (m, 3H, C*H*-6,5,3), 7.34 (s, 1H, C*H*-7), 6.10 (t, *J* = 2.0 Hz, 1H, C*H*-4''), 6.01 (d, *J* = 2.1 Hz, 2H, C*H*-2'',6''), 5.59 (s, 2H, O-CH_2-6'), 4.71 (t, *J* = 5.1 Hz, 2H, N–CH_2-7'), 4.31 (t, *J* = 5.0 Hz, 2H, O-CH_2-8'), 3.74 (s, 6H, O-CH_3-7'',8'').

^{13}C NMR (151 MHz, Chloroform-*d*): δ 161.61 (*C*q-3'',5''), 159.60 (*C*q-1''), 149.10 (*C*-2), 136.03 (*C*-4), 126.83 (*C*-6),124.39 (*C*-5' triazole), 121.57 (*C*-3), 120.26 (*C*-5), 110.19 (*C*-7), 93.93 (*C*-4''), 93.47 (*C*-2'',6''), 66.18 (O-*C*-8'), 62.96 (O-*C*-6'), 55.41 (O-*C*-7'',8''), 49.74 (N–*C*-7'). Not observed (*C*q-8, 8a,4a)

HRMS: (ESI$^+$-MS, *m/z*) calcd for $C_{22}H_{22}N_4O_4$ $(M+Na)^+$: 429.1539, found: 429.1542.

8-((1-(2-(o-tolyloxy)ethyl)-1H-1,2,3-triazol-4-yl)methoxy)quinoline (10 m) Beige solid; Yield: 69%; Chemical formula: $C_{21}H_{20}N_4O_2$; Mol. wt: 360.41 g/mol; R_f: 0.22 (EtOAc-Hexane, 80:20); mp: 98–100 °C.

^{1}H NMR (400 MHz, Chloroform-*d*): δ 8.93 (s, 1H, C*H*-2), 8.13 (s, 1H, C*H*-4), 7.94 (s, 1H, C*H*-5' triazole), 7.50–7.26 (m, 4H, C*H*-6,5,3,7), 7.15–7.01 (m, 2H, C*H*-5'',3''), 6.85 (t, *J* = 7.4 Hz, 1H, C*H*-4''), 6.70 (d, *J* = 8.0 Hz, 1H, C*H*-6''), 5.60 (s, 2H, O-CH_2-6'), 4.74 (t, *J* = 5.0 Hz, 2H, N–CH_2-7'), 4.31 (t, *J* = 5.0 Hz, 2H, O-CH_2-8'), 2.02 (s, 3H, Ph-CH_3-7'').

^{13}C NMR (101 MHz, Chloroform-*d*): δ 155.81 (*C*q-1''), 153.90 (*C*q-8), 144.22 (*C*q-4' triazole), 140.32 (*C*q-8a), 135.85 (*C*-4), 130.90 (*C*-3''), 126.84 (*C*-5''), 126.79 (*C*-6), 126.69 (*C*q-2''), 124.48 (*C*-5' triazole), 121.28 (*C*-4''), 110.84 (*C*-6''), 109.92 (*C*-7), 66.12 (O-*C*-8'), 62.80 (O-*C*-6'), 49.96 (N–*C*-7'), 16.15 (Ph-*C*-7''). Not observed (*C*-2,4a,5,3).

HRMS: (ESI$^+$-MS, *m/z*) calcd for $C_{21}H_{20}N_4O_2$ $(M+Na)^+$: 383.1484, found: 383.1491.

8-((1-(2-(m-tolyloxy)ethyl)-1H-1,2,3-triazol-4-yl)methoxy)quinoline (10n) Beige solid; Yield: 75%; Chemical formula: $C_{21}H_{20}N_4O_2$; Mol. wt: 360.41 g/mol; R_f : 0.22 (EtOAc-Hexane, 80:20); mp: 90–92 °C.

^{1}H NMR (600 MHz, Chloroform-*d*): δ 8.93 (s, 1H, C*H*-2), 8.13 (s, 1H, C*H*-4), 7.95 (s, 1H, C*H*-5' triazole), 7.47–7.36 (m, 3H, C*H*-6,5,3), 7.35–7.29 (m, 1H, C*H*-7), 7.11 (t, *J* = 7.9 Hz, 1H, C*H*-5''), 6.76 (d, *J* = 7.5 Hz, 1H, C*H*-4''), 6.63 (t, *J* = 2.0 Hz, 1H, C*H*-2''), 6.59 (dd, *J* = 8.2, 2.5 Hz, 1H, C*H*-6''), 5.58 (s, 2H, O-CH_2-6'), 4.70 (t, *J* = 5.1 Hz, 2H, N–CH_2-7'), 4.31 (t, *J* = 5.0 Hz, 2H, O-CH_2-8'), 2.28 (s, 3H, Ph-*C*-7'').

^{13}C NMR (151 MHz, Chloroform-*d*): δ 157.74 (*C*q-1''), 153.90 (*C*q-8), 149.24 (*C*-2), 144.21 (*C*q-4' triazole), 140.43 (*C*q-8a), 139.70 (*C*q-3''), 135.93 (*C*-4), 129.48 (*C*q-4a), 129.30 (*C*-5''), 126.78 (*C*-6), 124.45 (*C*-5' triazole), 122.47 (*C*-4''), 121.46 (*C*-3), 120.26 (*C*-5), 115.48 (*C*-2''), 111.33 (*C*-6''), 110.08 (*C*-7), 66.09 (O-*C*-8'), 62.94 (O-*C*-6'), 49.82 (N–*C*-7'), 21.42(Ph-*C*-7'').

HRMS: (ESI$^+$-MS, *m/z*) calcd for $C_{21}H_{20}N_4O_2$ $(M+Na)^+$: 383.1484, found: 383.1489.

8-((1-(2-(3,5-dimethylphenoxy)ethyl)-1H-1,2,3-triazol-4-yl)methoxy)quinoline (10q) Brown solid; Yield: 50%; Chemical formula: $C_{22}H_{22}N_4O_2$; Mol. wt: 374.44 g/mol; R_f: 0.20 (EtOAc-Hexane, 80:20). mp: 92–94 °C.

^{1}H NMR (600 MHz, Chloroform-*d*): δ 8.95 (s, 1H, C*H*-2), 8.14 (s, 1H, C*H*-4), 7.96 (s, 1H, C*H*-5' triazole), 7.50–7.36 (m, 3H, C*H*-6,5,3), 7.34 (s, 1H, C*H*-7), 6.61 (s, 1H, C*H*-4''), 6.45 (s, 2H, C*H*-2'',6''), 5.59 (s, 2H, O-CH_2-6'), 4.70 (t, *J* = 5.0 Hz, 2H, N-CH_2-7'), 4.31 (t, *J* = 5.0 Hz, 2H, O-CH_2-8'), 2.25 (s, 6H, Ph-CH_3-7'',8'').

^{13}C NMR (151 MHz, Chloroform-*d*): δ 157.76 (*C*q-1''), 153.92 (*C*q-8), 149.26 (*C*-2), 144.21 (*C*q-4' triazole), 140.27 (*C*q-8a), 139.41 (*C*q-3'',5''), 135.98 (*C*-4), 129.50 (*C*q-4a), 126.81 (*C*-6), 124.45 (*C*-5' triazole), 123.40 (*C*-4''), 121.63 (*C*-3), 120.19 (*C*-5), 112.31 (*C*-2'',6''), 110.16 (*C*-7), 66.03 (O-*C*-8'), 62.97 (O-*C*-6'), 49.85 (N-*C*-7'), 21.35 (Ph-*C*-7'',8'').

5-(2-(4-((quinolin-8-yloxy)methyl)-1H-1,2,3-triazol-1-yl)ethoxy)benzene-1,3-diol (10v) Beige solid; Yield: 50%; Chemical formula: $C_{20}H_{18}N_4O_4$; Mol. wt: 378.38 g/mol; R_f : 0.07 (EtOAc-Hexane, 80:20). mp: 197–199 °C

^{1}H NMR (600 MHz, DMSO-d_6): δ 9.21 (s, 2H, O*H*-7'',8''), 8.84 (d, *J* = 4.3 Hz, 1H, C*H*-2), 8.35 (s, 1H, C*H*-5' triazole), 8.32 (dd, *J* = 8.2, 1.7 Hz, 1H, C*H*-4), 7.57–7.50 (m,

3H, C*H*-6,5,3), 7.42 (dd, *J* = 6.5, 2.4 Hz, 1H, C*H*-7), 5.86 (t, *J* = 2.0 Hz, 1H, C*H*-4''), 5.81 (d, *J* = 2.0 Hz, 2H, C*H*-2'',6''), 5.37 (s, 2H, O-CH_2-6'), 4.76 (t, *J* = 5.1 Hz, 2H, N-CH_2-7''), 4.29 (t, *J* = 5.2 Hz, 2H, O-CH_2-8').

^{13}C NMR (151 MHz, DMSO-d_6): δ 159.57 (*C*q-1''), 159.03 (*C*q-3'',5''), 153.87 (*C*q-8), 148.96 (*C*-2), 142.63 (*C*q-4' triazole), 139.77 (*C*q-8a), 135.75 (*C*-4), 129.06 (*C*q-4a), 126.70 (*C*-6), 125.21 (*C*-5' triazole), 121.81 (*C*-3), 120.03 (*C*-5), 110.15 (*C*-7), 96.01 (*C*-4''), 93.28 (*C*-2'',6''), 65.80 (O-*C*-8'), 61.90 (O-*C*-6'), 49.08 (N-*C*-7').

HRMS: (ESI^+-MS, *m/z*) calcd for $C_{20}H_{18}N_4O_4$ $(M+Na)^+$: 401.1226, found: 401.1229.

8-((1-(2-(naphthalen-2-yloxy)ethyl)-1H-1,2,3-triazol-4-yl)methoxy)quinoline (10z) Beige solid; Yield: 50%; Chemical formula: $C_{24}H_{20}N_4O_2$; Mol. wt: 396.44 g/mol; R_f: 0.20 (EtOAc-Hexane, 80:20); mp: 123–125 °C.

^{1}H NMR (400 MHz, Chloroform-*d*): δ 8.92 (s, 1H, C*H*-2), 8.12 (s, 1H, C*H*-4), 7.99 (s, 1H, C*H*-5' triazole), 7.73 (d, *J* = 8.1 Hz, 1H, C*H*-5''), 7.70–7.64 (m, 2H, C*H*-4'',8''), 7.47–7.29 (m, 6H, C*H*-7'',6,5,3,7,6''), 7.04 (d, *J* = 2.3 Hz, 1H, C*H*-1''), 7.01 (dd, *J* = 8.8, 2.5 Hz, 1H, C*H*-3''), 5.58 (s, 2H, OCH_2-6'), 4.75 (t, *J* = 5.0 Hz, 2H, NCH_2-7'),4.41 (t, *J* = 4.9 Hz, 2H, OCH_2-8').

^{13}C NMR (101 MHz, Chloroform-*d*): δ 155.63 (*C*q-2''), 144.24 (*C*q-4' triazole), 135.84 (*C*-4), 134.25 (*C*q-8''a), 129.68 (*C*-4''), 129.27 (*C*q-4''a), 127.64 (*C*-5''), 126.81 (*C*-8''), 126.57 (*C*-7''), 124.50 (*C*-5' triazole), 124.07 (*C*-6''), 118.37 (*C*-3''), 109.86 (*C*-7), 106.99 (*C*-1''), 66.15 (O-*C*-8'), 62.83 (O-*C*-6'), 49.74 (N-*C*-7'). Not observed (C-8,2,8a,4a,6,5,3).

HRMS: (ESI^+-MS, *m/z*) calcd for $C_{21}H_{18}N_4O_3$ $(M+Na)^+$: 419.1484, found: 419.1494.

N-(2-(4-((quinolin-8-yloxy)methyl)-1H-1,2,3-triazol-1-yl)ethyl)aniline (11a) Off-white solid; Yield: 51%; Chemical formula: $C_{20}H_{19}N_5O$; Mol. wt: 345.40 g/mol; R_f: 0.20 (EtOAc-Hexane, 80:20); mp: 96–98 °C

^{1}H NMR (600 MHz, Chloroform-*d*): δ 8.93 (s, 1H, C*H*-2), 8.15 (s, 1H, C*H*-4), 7.74 (s, 1H, C*H*-5' triazole), 7.49–7.39 (m, 3H, C*H*-6,5,3), 7.31 (s, 1H, C*H*-7), 7.13 (dd, *J* = 8.5, 7.2 Hz, 2H, C*H*-3'',5''), 6.71 (t, *J* = 7.3 Hz, 1H, C*H*-4''), 6.54 (dd, *J* = 8.5, 1.2 Hz, 2H, C*H*-2'',6''), 5.56 (s, 2H, O-CH_2-6'), 4.52 (dd, *J* = 6.5, 4.9 Hz, 2H, N-CH_2-7'), 3.65 (t, *J* = 5.7 Hz, 2H, N-CH_2-8'). Not observed (N*H*-9').

^{13}C NMR (151 MHz, Chloroform-*d*): δ 153.82 (*C*q-8), 149.24 (*C*-2), 146.59 (*C*q-1''), 144.15 (*C*q-4' triazole), 140.18 (*C*q-8a), 136.08 (*C*-4), 129.62 (*C*q-4a), 129.45 (*C*-3'',5''), 126.82 (*C*-6), 124.12 (*C*-5' triazole), 121.68 (*C*-3), 120.26 (*C*-5), 118.30 (*C*-4''), 113.00 (*C*-2'',6''), 110.00 (*C*-7), 62.89 (O-*C*-6'), 49.33 (N-*C*-7'), 43.66 (N-*C*-8').

HRMS: (ESI^+-MS, *m/z*) calcd for $C_{20}H_{19}N_5O$ $(M+Na)^+$: 368.1487, found: 368.1486.

2-chloro-N-(2-(4-((quinolin-8-yloxy)methyl)-1H-1,2,3-triazol-1-yl)ethyl)aniline (11d) Brown solid; Yield: 53%; Chemical formula: $C_{20}H_{18}ClN_5O$; Mol. wt: 379.84 g/mol; R_f: 0.24 (EtOAc-Hexane, 80:20); mp: 118–120 °C.

^{1}H NMR (600 MHz, Chloroform-*d*): δ 8.85 (d, *J* = 4.7 Hz, 1H, C*H*-2), 8.04 (dd, *J* = 8.1, 1.7 Hz, 1H, C*H*-4), 7.70 (s, 1H, C*H*-5'triazole), 7.41–7.30 (m, 3H, C*H*-6,5,3), 7.22 (dd, *J* = 7.2, 1.6 Hz, 1H, C*H*-7), 7.15 (dd, *J* = 7.9, 1.5 Hz, 1H, C*H*-3''), 7.02 (td, *J* = 7.8, 1.5 Hz, 1H, C*H*-5''), 6.56 (td, *J* = 7.7, 1.4 Hz, 1H, C*H*-4''), 6.52 (dd, *J* = 8.2, 1.4 Hz, 1H, C*H*-6''), 5.46 (s, 2H, O-CH_2-6'), 4.55 (t, *J* = 6.4 Hz, 1H, N*H*-9'), 4.45 (t, *J* = 5.9 Hz, 2H, N-CH_2-7'), 3.63 (q, *J* = 5.9 Hz, 2H, N-CH_2-8').

^{13}C NMR (151 MHz, Chloroform-*d*): δ 153.80 (*C*q-8), 149.21 (*C*-2), 144.10 (*C*q-4' triazole), 142.62 (*C*q-1''), 140.26 (*C*q-8a), 135.93 (*C*-4), 129.46 (*C*q-4a), 129.42 (*C*-3''), 127.84 (*C*-5''), 126.69 (*C*-6), 124.14 (*C*-5' triazole), 121.60 (*C*-3), 120.22 (*C*-5), 119.54 (*C*q-2''), 118.11 (*C*-4''), 110.91 (*C*-6''), 109.93 (*C*-7), 62.75 (O-*C*-6'), 49.16 (N-*C*-7'), 43.30 (N-*C*-8').

HRMS: (ESI^+-MS, *m/z*) calcd for $C_{20}H_{18}ClN_5O$ $(M+Na)^+$: 402.1098, found: 402.1102.

4.2.18 8-((1-phenethyl-1H-1,2,3-triazol-4-yl)methoxy) quinoline (14) Brown solid; Yield: 51%; Chemical formula: $C_{20}H_{18}N_4O$; Mol. wt: 330.38 g/mol; R_f: 0.23 (EtOAc-Hexane, 80:20); mp: 70–72 °C.

^{1}H NMR (600 MHz, Chloroform-*d*): δ 8.90 (s, 1H, C*H*-2), 8.11 (d, *J* = 8.2 Hz, 1H, C*H*-4), 7.48 (s, 1H, C*H*-5' triazole), 7.43–7.35 (m, 3H, C*H*-6,5,3), 7.25 (d, *J* = 6.8 Hz, 1H, C*H*-7), 7.15–7.09 (m, 3H, C*H*-11',13',12'), 6.99 (dd, *J* = 7.7, 1.7 Hz, 2H, C*H*-10',14'), 5.51 (s, 2H, O-CH_2-6'), 4.52 (t, *J* = 7.3 Hz, 2H, N-CH_2-7'), 3.14 (t, *J* = 7.3 Hz, 2H, Ph-CH_2-8').

^{13}C NMR (151 MHz, Chloroform-*d*): δ 153.78 (*C*q-8), 149.22 (*C*-2), 143.86 (*C*q-4' triazole), 140.29 (*C*q-8a), 136.83 (*C*q-9'), 136.00 (*C*-4), 129.48 (*C*q-4a), 128.70 (*C*-11',13'), 128.56 (*C*-10',14'), 127.00 (*C*-12'), 126.76 (*C*-6), 123.47 (*C*-5' triazole), 121.59 (*C*-3), 120.15 (*C*-5), 109.99 (*C*-7), 62.87 (O-*C*-6'), 51.66 (N-*C*-7'), 36.61 (Ph-*C*-8').

HRMS: (ESI^+-MS, *m/z*) calcd for $C_{20}H_{18}N_4O$ $(M+Na)^+$: 353.1378, found: 353.1384.

4.2.19 2-(4-((quinolin-8-yloxy)methyl)-1H-1,2,3-triazol-1-yl)ethanol (15) Brown solid; Yield: 60%; Chemical formula: $C_{14}H_{14}N_4O_2$; Mol. wt: 270.29 g/mol; R_f: 0.05 (EtOAc-Hexane, 80:20); 0.17 (EtOAc–MeOH, 98:2); mp: 140–142 °C

^{1}H NMR (400 MHz, Chloroform-*d*): δ 8.82 (dd, *J* = 4.4, 1.7 Hz, 1H, C*H*-2), 8.11 (dd, *J* = 8.3, 1.7 Hz, 1H, C*H*-4), 7.94 (s, 1H, C*H*-5' triazole), 7.47–7.35 (m, 3H, C*H*-6,5,3), 7.27 (dd, *J* = 7.4, 1.6 Hz, 1H, C*H*-7), 5.44 (s, 2H, O-CH_2-6'), 4.45 (dd, *J* = 5.7, 3.9 Hz, 2H, N–CH_2-7'), 4.00 (t, *J* = 5.0 Hz, 2H, CH_2-8'), Not observed (OH-9').

^{13}C NMR (101 MHz, Chloroform-*d*): δ 153.76 (*C*q-8), 149.12 (*C*-2), 143.69 (*C*q-4' triazole), 140.00 (*C*q-8a), 136.16 (*C*-4), 129.48 (*C*q-4a), 126.80 (*C*-6), 124.66 (*C*-5' triazole), 121.67 (*C*-3), 120.16 (*C*-5), 109.74 (*C*-7), 62.72 (O-*C*-6'), 61.00 (*C*-8'), 52.82 (N–*C*-7').

2-(4-((quinolin-8-yloxy)methyl)-1H-1,2,3-triazol-1-yl) ethyl 4-methylbenzenesulfonate (16) Pale-yellow oil; Yield: 71%; Chemical formula: $C_{14}H_{14}N_4O_2$; Mol. wt: 424.47 g/mol; R_f : 0.20 (EtOAc-Hexane, 80:20).

^{1}H NMR (600 MHz, Chloroform-*d*): δ 8.94 (d, $J = 3.2$ Hz, 1H, C*H*-2), 8.15 (d, $J = 8.2$ Hz, 1H, C*H*-4), 7.85 (s, 1H, C*H*-5' triazole), 7.65 (d, $J = 8.3$ Hz, 2H, C*H*-3'',5''), 7.49–7.40 (m, 3H, C*H*-6,5,3), 7.31 (d, $J = 7.5$ Hz, 1H, C*H*-7), 7.24 (d, $J = 8.0$ Hz, 2H, C*H*-2'',6''), 5.51 (s, 2H, O-CH_2-6'), 4.60 (t, $J = 5.2$ Hz, 2H, N-CH_2-7'), 4.40 (t, $J = 5.2$ Hz, 2H, O-CH_2-8'), 2.38 (s, 3H, Ph-CH_3-7'').

^{13}C NMR (151 MHz, Chloroform-*d*): δ 153.81 (*C*q-8), 149.25 (*C*-2), 145.38 (*C*q-1''), 144.28 (*C*q-4' triazole), 140.16 (*C*q-8a), 136.16 (*C*-4), 132.11 (*C*q-4''), 130.01 (*C*-3'',5''), 129.54 (*C*q-4a), 127.83 (*C*-2'',6''), 126.79 (*C*-6), 124.39 (*C*-5' triazole), 121.67 (*C*-3), 120.35 (*C*-5), 110.16 (*C*-7), 67.32 (O-*C*-8'), 62.84 (O-*C*-6'), 49.09 (N-*C*-7'), 21.59 (Ph-C-7'').

8-(2-(p-tolyloxy)ethoxy)quinoline (17) Beige solid; Yield: 91%; Chemical formula: $C_{18}H_{17}NO_2$; Mol. wt: 279.33 g/mol; R_f : 0.60 (EtOAc-hexane 80:20); mp: 132–134 °C

^{1}H NMR (400 MHz, Chloroform-*d*) δ 8.98 (dd, $J = 4.3$, 1.7 Hz, 1H, C*H*-2), 8.17 (dd, $J = 8.3$, 1.7 Hz, 1H, C*H*-4), 7.54–7.40 (m, 3H, C*H*-6,5,3), 7.20 (dd, $J = 7.5$, 1.5 Hz, 1H, C*H*-7), 7.09 (d, $J = 8.7$ Hz, 2H, C*H*-13,14), 6.88 (d, $J = 8.6$ Hz, 2H, C*H*-12,16), 4.63 (t, $J = 5.3$ Hz, 2H, O-CH_2-9), 4.54 (t, $J = 5.3$ Hz, 2H, O-CH_2-10), 2.29 (s, 3H, Ph-CH_3-17).

^{13}C NMR (101 MHz, Chloroform-*d*) δ 156.46 (*C*q-11), 154.48 (*C*q-8), 149.35 (*C*-2), 140.27 (*C*q-8a), 136.12 (*C*-4), 130.34 (*C*q-14), 129.96 (*C*-13,15), 129.60 (*C*q-4a), 126.71 (*C*-6), 121.68 (*C*-3), 120.23 (*C*-5), 114.58 (*C*-12,16), 109.55 (*C*-7), 67.41 (O-*C*-9), 66.37 (O-*C*-10), 20.50 (Ph-*C*-17).

LRMS: (ESI$^+$-MS, m/z) $C_{18}H_{17}NO_2$ $(M + Na)^+$: 302.1315.

8-phenethoxyquinoline (18) Pale-yellow oil; Yield: 90%; Chemical formula: $C_{17}H_{15}NO$; Mol. wt: 249.31; R_f : 0.61 (EtOAc-hexane 80:20).

^{1}H NMR (400 MHz, Chloroform-*d*) δ 8.88 (dd, $J = 4.2$, 1.7 Hz, 1H, C*H*-2), 8.03 (dd, $J = 8.3$, 1.7 Hz, 1H, C*H*-4), 7.40–7.21 (m, 8H, C*H*-6,5,3,12,13,14,15,16), 6.96 (dd, $J = 7.5$, 1.4 Hz, 1H, C*H*-7), 4.34 (t, $J = 7.7$ Hz, 2H, C*H*-9), 3.28 (t, $J = 7.7$ Hz, 2H, C*H*-10).

^{13}C NMR (101 MHz, Chloroform-*d*) δ 153.49 (Cq-8), 148.28 (C-2), 139.30 (Cq-8a), 136.78 (Cq-11), 134.90 (C-4), 128.50 (Cq-4a), 128.07 (C-12,16), 127.56 (C-13,15), 125.62 (C-6), 125.56 (C-14), 120.55 (C-3), 118.67 (C-5), 107.81 (C-7), 68.75 (C-9), 34.61 (C-10).

HRMS: (ESI$^+$-MS, *m/z*) calcd for $C_{17}H_{15}NO$ $(M + Na)^+$: 272.1051, found: 272.1046.

In vitro bioassays

Sample preparation

Samples of examined hybrids were stored frozen at − 20 °C and then prepared in DMSO and water to a final concentration of 32 µg/mL in 384-well plates for the preliminary screening phase. For the hit-confirmation phase, they were further diluted serially 1:2-fold for eight times. The concentration was prepared in a non-binding surface plate (NBS) for bacterial and fungal strains, tissue-culture-treated black wall/clear bottom for mammalian cell types (cytotoxicity assay), and polypropylene 384-well for hemolysis assays. The preparation was done in duplicates ($n = 2$) while keeping the final concentration of DMSO to 1% DMSO for preliminary antimicrobial screening phase and 0.5% for the hit-confirmation phase, cytotoxicity, and hemolytic assays.

Antibacterial assay

Selected bacteria strains were cultured in Cation-adjusted Mueller–Hinton broth at 37 °C overnight, followed by diluting each culture sample by 40-fold in fresh broth and incubating at 37 °C for 1.5–3 h. After that, the resultant mid-log phase cultures were diluted (CFU/mL measured by OD_{600}) and added to each well plate containing the compounds to give a cell density of 5×10^5 CFU/mL and a total volume of 50 µL. The plates were then covered and incubated at 37 °C for 18 h without shaking.

To determine the inhibition of bacterial growth, a Tecan M1000 Pro monochromator plate reader was used to measure the absorbance at 600 nm (OD_{600}) and subsequently the percentage growth inhibition was calculated for each well using the negative control (media only) and positive control (bacteria without inhibitors) on the same plate as references. The MIC was then determined as the lowest concentration causing full growth inhibition, i.e., ≥ 80% inhibition.

Antifungal assay

Antifungal activity was determined by culturing the fungi strains on a Yeast Extract-Peptone Dextrose (YPD) agar for three days at 30 °C. Then, a yeast suspension of 1×10^6 to 5×10^6 CFU/mL was prepared from five colonies, and the suspension was diluted and added to each well plate containing the compound to give a final cell density of fungi

suspension of 2.5×10^3 CFU/mL and a total volume of 50 µL. All plates were covered and incubated at 35 °C for 36 h without shaking.

Analysis of fungi growth inhibition was achieved using Biotek Multiflo Synergy HTX plate reader to measure the absorbance at 630 nm (OD_{630}) for *C. albicans*, while the difference in absorbance between 600 and 570 nm ($OD_{600\text{-}570}$) was determined for *C. neoformans*, both after the addition of resazurin (0.001% final concentration) and incubation at 35 °C for 2 h. The percentage inhibition was determined as in antibacterial assay.

Cytotoxicity assay

HEK293 cells (ATCC CRL-1573) were counted manually in a Neubauer hemocytometer and then plated in the well plates containing the hit compounds (≥ 80% inhibition) to give a density of 5000 cells/well in a final volume of 50 µL. The utilized growth media was a Dulbecco's modified eagle medium supplemented with 10% fetal bovine serum (from GE Healthcare Australia; cat #SH30084.03). The cells and the compounds were incubated at 37 °C for 20 h in 5% CO_2.

Subsequently, cytotoxicity was determined by measuring the fluorescence intensity at 560/10 nm and 590/10 nm ($F_{560/590}$) as excitation and emission wavelengths, respectively, using a Tecan M1000 Pro monochromator plate reader and automatic gain calculation, after the addition of 5 µL of 25 µg/mL resazurin (2.3 µg/mL final concentration) and another 3-h incubation at 37 °C in 5% CO_2. The concentration at 50% cytotoxicity (CC_{50}) was then calculated by curve fitting the inhibition values *vs.* log(concentration) using a sigmoidal dose–response function implemented in Pipeline Pilot's dose–response component.

Hemolysis assay

Human whole blood (from Australian Red Cross Life Blood) was washed three times with 3 volumes of 0.9% NaCl and resuspended in the same to a concentration of 0.5×10^8 cells/mL using manual cell count in a Neubauer hemocytometer. Subsequently, the washed cells were transferred to the well plates containing the compounds for a final volume of 50 µL, followed by shaking the plates for 10 min on a plate shaker. After this, the plates were incubated at 37 °C for 1 h, centrifuged at 1000 g for 10 min to pellet cells and debris, and then, 25 µL of the supernatant was transferred to a polystyrene 384-well assay plate.

Hemolysis was determined by measuring the absorbance of the resulting supernatant at 405 mm (OD_{405}) with a Tecan M1000 Pro monochromator plate reader. HC_{10} and HC_{50} (concentrations at 10% and 50% hemolysis, respectively) were calculated as in cytotoxicity assay above.

In silico procedures

The X-ray crystal structure and experimental density of selected proteins were refined using PrimeX 5.6 [33], before docking simulations. Subsequently, the refined protein structure was prepared with the Protein Preparation Wizard [34]. This approach allowed the controlled minimization of protein structure for high energy contacts, improper binding site packing, and other shortfalls inherited from the experimental crystal data. Moreover, considering the importance of accounting for protein flexibility to accurate prediction of protein–ligand interactions, induced-fit docking protocol [35] was employed to study the behavior of compound **16** and other potent hybrids in the active sites of selected antimicrobial targets. 3D structures of all ligands were prepared with LigPrep [36], while their ionization states were assigned at pH 7.0 ± 2.0 using Epik [37]. The overall workflow adopted for the in silico studies is provided in the Online Resource (Fig. S2).

Acknowledgements PS thanks the National Research Foundation of South Africa for a Competitive Grant for unrated Researchers (Grant No. 121276). We also appreciate the Centre for High-Performance Computing (CHPC), Cape Town for computational resources, and the Community for Antimicrobial Drug Discovery (CO-ADD), funded by the Wellcome Trust (UK) and the University of Queensland (Australia) for antimicrobial screening.

Compliance with ethical standards

Conflict of interest The authors declare that they have no conflict of interest.

Ethics approval Ethics approval for the hemolysis assay is The University of Queensland Institutional Human Research Ethics Approval approved by the Medical Research Ethics Committee.

References

1. Brown ED, Wright GD (2016) Antibacterial drug discovery in the resistance era. Nature 529(7586):336–343. https://doi.org/10.1038/nature17042
2. Morens DM, Fauci AS (2013) Emerging infectious diseases: threats to human health and global stability. PLoS Pathog 9(7):e1003467. https://doi.org/10.1371/journal.ppat.1003467
3. Lesho EP, Laguio-Vila M (2019) The slow-motion catastrophe of antimicrobial resistance and practical interventions for all prescribers. In: Mayo Clinic proceedings. Elsevier
4. Croston GE (2017) The utility of target-based discovery. Expert Opin Drug Dis 12(5):427–429. https://doi.org/10.1080/17460441.2017.1308351
5. Morphy JR, Harris CJ (eds) (2012) Designing multi-target drugs, vol 21. Royal society of chemistry. RSC Drug Discovery, Cambridge

6. Shaveta MS, Singh P (2016) Hybrid molecules: the privileged scaffolds for various pharmaceuticals. Eur J Med Chem 124:500–536. https://doi.org/10.1016/j.ejmech.2016.08.039
7. Zhang B (2019) Comprehensive review on the anti-bacterial activity of 1,2,3-triazole hybrids. Eur J Med Chem 168:357–372. https://doi.org/10.1016/j.ejmech.2019.02.055
8. Xu Z, Zhao SJ, Liu Y (2019) 1,2,3-Triazole-containing hybrids as potential anticancer agents: current developments, action mechanisms and structure-activity relationships. Eur J Med Chem 183:111700. https://doi.org/10.1016/j.ejmech.2019.111700
9. Aneja B, Azam M, Alam S, Perwez A, Maguire R, Yadava U, Kavanagh K, Daniliuc CG, Rizvi MMA, Haq QMR (2018) Natural product-based 1, 2, 3-triazole/sulfonate analogues as potential chemotherapeutic agents for bacterial infections. ACS Omega 3(6):6912–6930. https://doi.org/10.1021/acsomega.8b00582
10. Bonandi E, Christodoulou MS, Fumagalli G, Perdicchia D, Rastelli G, Passarella D (2017) The 1,2,3-triazole ring as a bioisostere in medicinal chemistry. Drug Discov Today 22(10):1572–1581. https://doi.org/10.1016/j.drudis.2017.05.014
11. Irfan M, Alam S, Manzoor N, Abid M (2017) Effect of quinoline based 1,2,3-triazole and its structural analogues on growth and virulence attributes of *Candida albicans*. PLoS ONE 12(4):1–23. https://doi.org/10.1371/journal.pone.0175710
12. Irfan M, Aneja B, Yadava U, Khan SI, Manzoor N, Daniliuc CG, Abid M (2015) Synthesis, QSAR and anticandidal evaluation of 1,2,3-triazoles derived from naturally bioactive scaffolds. Eur J Med Chem 93:246–254. https://doi.org/10.1016/j.ejmech.2015.02.007
13. Xu Z, Zhang S, Song X, Qiang M, Lv Z (2017) Design, synthesis and in vitro anti-mycobacterial evaluation of gatifloxacin-1H-1, 2, 3-triazole-isatin hybrids. Bioorg Med Chem Lett 27(16):3643–3646. https://doi.org/10.1016/j.bmcl.2017.07.023
14. Xu Z, Lv ZS, Song XF, Qiang M (2017) Ciprofloxacin-isatin-1H-1,2,3-triazole hybrids: design, synthesis, and in vitro anti-tubercular activity against *M. Tuberculosis*. J Heterocycl Chem 55(1):97–102. https://doi.org/10.1002/jhet
15. Kant R, Kumar D, Agarwal D, Gupta RD, Tilak R, Awasthi SK, Agarwal A (2016) Synthesis of newer 1,2,3-triazole linked chalcone and flavone hybrid compounds and evaluation of their antimicrobial and cytotoxic activities. Eur J Med Chem 113:34–49. https://doi.org/10.1016/j.ejmech.2016.02.041
16. Gao F, Ye L, Kong F, Huang G, Xiao J (2019) Design, synthesis and antibacterial activity evaluation of moxifloxacin-amide-1,2,3-triazole-isatin hybrids. Bioorg Chem 91:103162. https://doi.org/10.1016/j.bioorg.2019.103162
17. Gao F, Chen Z, Ma L, Fan Y, Chen L, Lu G (2019) Synthesis and biological evaluation of moxifloxacin-acetyl-1,2,3-1*H*-triazole-methylene-isatin hybrids as potential anti-tubercular agents against both drug-susceptible and drug-resistant *Mycobacterium tuberculosis* strains. Eur J Med Chem 180:648–655. https://doi.org/10.1016/j.ejmech.2019.07.057
18. Song Yn X, Chen W, Zhan P, Liu X (2015) 8-Hydroxyquinoline: a privileged structure with a broad-ranging pharmacological potential. MedChemComm 6(1):61–74. https://doi.org/10.1039/c4md00284a
19. Oliveri V, Vecchio G (2016) 8-Hydroxyquinolines in medicinal chemistry: a structural perspective. Eur J Med Chem 120:252–274. https://doi.org/10.1016/j.ejmech.2016.05.007
20. Awolade P, Cele N, Kerru N, Gummidi L, Oluwakemi E, Singh P (2020) Therapeutic significance of β-glucuronidase activity and its inhibitors: a review. Eur J Med Chem 187:111921. https://doi.org/10.1016/j.ejmech.2019.111921
21. CLH (2014) CLH report for 8-hydroxyquinoline
22. Ebenezer O, Awolade P, Koorbanally N, Singh P (2020) New library of pyrazole-imidazo[1,2-α]pyridine molecular conjugates: synthesis, antibacterial activity and molecular docking studies. Chem Biol Drug Des 95:162–173. https://doi.org/10.1111/cbdd.13632
23. Ebenezer O, Singh-Pillay A, Koorbanally NA, Singh P (2020) Antibacterial evaluation and molecular docking studies of pyrazole–thiosemicarbazones and their pyrazole–thiazolidinone conjugates. Mol Divers. https://doi.org/10.1007/s11030-020-10046-w
24. Das B, Venkateswarlu K, Majhi A, Siddaiah V, Reddy KR (2007) A facile nuclear bromination of phenols and anilines using NBS in the presence of ammonium acetate as a catalyst. J Mol Catal A Chem 267(1–2):30–33. https://doi.org/10.1016/j.molcata.2006.11.002
25. Lim JY, Marques I, Thompson AL, Christensen KE, Felix V, Beer PD (2017) Chalcogen bonding macrocycles and [2]rotaxanes for anion recognition. J Am Chem Soc 139(8):3122–3133. https://doi.org/10.1021/jacs.6b12745
26. Helsel ME, White EJ, Razvi SZA, Alies B, Franz KJ (2017) Chemical and functional properties of metal chelators that mobilize copper to elicit fungal killing of *Cryptococcus neoformans*. Metallomics 9(1):69–81. https://doi.org/10.1039/C6MT00172F
27. Kerns EH, Di L (2008) Drug-like properties: concepts, structure design and methods: from ADME to toxicity optimization, 1st edn. Elsevier, Amsterdam
28. QikProp (2019) QikProp, version 6.0. Schrödinger, LLC, New York
29. Hall ML, Jorgensen WL, Whitehead L (2013) Automated ligand- and structure-based protocol for in silico prediction of human serum albumin binding. J Chem Inf Model 53(4):907–922. https://doi.org/10.1021/ci3006098
30. Vandenberg JI, Perry MD, Perrin MJ, Mann SA, Ke Y, Hill AP (2012) hERG K(+) channels: structure, function, and clinical significance. Physiol Rev 92(3):1393–1478. https://doi.org/10.1152/physrev.00036.2011
31. Hering J, Dunevall E, Ek M, Branden G (2018) Structural basis for selective inhibition of antibacterial target MraY, a membrane-bound enzyme involved in peptidoglycan synthesis. Drug Discov Today 23(7):1426–1435. https://doi.org/10.1016/j.drudis.2018.05.020
32. Sagatova AA, Keniya MV, Wilson RK, Monk BC, Tyndall JD (2015) Structural insights into binding of the antifungal drug fluconazole to *Saccharomyces cerevisiae* lanosterol 14α-demethylase. Antimicrob Agents Chemother 59(8):4982–4989. https://doi.org/10.1128/AAC.00925-15
33. PrimeX (2019) PrimeX version 5.6. Schrödinger, LLC, New York
34. Protein Preparation Wizard (2019) Protein Preparation Wizard; Epik, Schrödinger, LLC, New York, NY, 2019; Impact, Schrödinger, LLC, New York, NY, 2019; Prime, Schrödinger, LLC, New York, NY, 2019
35. Induced Fit Docking Protocol (2019) Induced Fit Docking protocol; Glide, Schrödinger, LLC, New York, NY, 2019; Prime, Schrödinger, LLC, New York, NY. 2019
36. LigPrep, Schrödinger, LLC, New York, NY. 2019. (2019)
37. Epik, Schrödinger, LLC, New York, NY. 2019. (2019)